Hydrogeology Journal (2020) 28:1635–1659
https://doi.org/10.1007/s10040-020-02128-8

REPORT

Hydrochemical and environmental isotopes analysis for characterizing a complex karst hydrogeological system of Watuputih area, Rembang, Central Java, Indonesia

Taat Setiawan[1,2] · Boy Yoseph C. S. S. Syah Alam[1] · Eko Haryono[3] · Hendarmawan[1]

Received: 9 May 2019 / Accepted: 3 February 2020 / Published online: 4 March 2020

Abstract

The karst hydrogeology systems of the Watuputih Hills region of Central Java, Indonesia, have many springs with varying discharge and are composed of formations with complex geological structures. This work characterized the karst hydrogeology by studying 50 hydrogeological features (caves, springs and wells) and by analyzing the chemical-physical properties of groundwater in the field (pH, temperature, EC, HCO_3^-, ^{222}Rn) and the major ions and stable isotopes of the groundwater samples in the laboratory, along with the stable isotope content of rainwater sampled over 1 year. Hierarchical cluster analysis of the water samples identified three hydrochemical groups: groundwater flowing through carbonate rocks (groups C2 and C3), through quartz sandstones and volcanic rocks (group C4), and through carbonate rocks and the siliciclastic rocks (quartz sandstones) underneath them (group C1). Springs with large discharge, typified as artesian fault-guided springs, were categorized into group C1. These springs are Sumbersemen, Brubulan Tahunan, and Brubulan Pesucen, with mean discharges of 1,516, 165, and 95 L/s, respectively. Based on the results of the stable isotope analysis, the d-excess calculation and the ^{222}Rn concentrations, groups C2, C3, and C4 associate with shallow groundwater systems that dominantly flow through pores, whereas group C1 associates with a deep groundwater system controlled by geological structure. The geological structure also determines the groundwater flow in the cave streams. The shallow groundwater system is sourced by local rainwater, while the deep groundwater system displays a relationship with the groundwater in the northern hills at an elevation >375 m above sea level.

Keywords Hydrochemistry · Stable isotopes · Radon · Karst · Indonesia

Introduction

Karst regions have a specific hydrogeological character (Milanovic 1981; Ford and Williams 1989, 2007) because the constituent rocks, like limestone and dolomite, are highly susceptible to chemical dissolution (Milanovic 1981; Goldscheider and Andreo 2007; Ford and Williams 1989, 2007). For karst regions, study of chemistry is essential (White 2015) because hydrochemical properties reflect the mechanism of groundwater flow in karstic rocks (Ford and Williams 1989; Ford and Williams 2007). Karst aquifers have heterogeneous characteristics owing to the three media-based systems through which groundwater flows, namely pores, fractures, and cavities (Goldscheider et al. 2007). In Indonesia, karst aquifers develop mainly in limestones and only occasionally in dolomite and marble, and these features have not been found in noncarbonate rocks (Haryono 2001).

This report elaborates on hydrochemical characteristics using hierarchical group analysis, which is validated with the data of stable isotopes (^{18}O, ^{2}H) and radon (^{222}Rn), to identify the karst hydrogeological system characteristics in Watuputih Hills and the surrounding areas. The area is located in Rembang Regency, Central Java Province, Indonesia, where active limestone mining of the Paciran Formation takes place. Since approximately 2014, the

✉ Taat Setiawan
taat.setiawan@esdm.go.id; taat17001@mail.unpad.ac.id; taat_setia@yahoo.com

[1] Faculty of Geological Engineering, Universitas Padjadjaran, Jatinangor, Sumedang 45363, Indonesia

[2] Center for Groundwater and Environmental Geology, Geological Agency, Ministry of Energy and Mineral Resources Republic of Indonesia, Diponegoro 57, Bandung 40122, Indonesia

[3] Faculty of Geography, Universitas Gadjah Mada, Bulaksumur, Yogyakarta 55281, Indonesia

study area has been heavily discussed due to the growing concerns of the community about the sustainability of springs connected to the limestone mining.

Studies of karst hydrogeological systems using hydrochemical and stable isotope analyses (^{18}O and ^{2}H) have been carried out by, for instance, Ashjari and Raeisi (2006), Petitta et al. (2011), Krishnaraj et al. (2012), Dimitriou and Tsintza (2015), and Thilakerathne et al. (2015), while more specific study employing multivariate hydrochemical analysis has also been conducted by, e.g., Valdes et al. (2007), Narany et al. (2014), Chihi et al. (2015), and Yuan et al. (2017). These previous studies generally explain hydrochemical processes such as dissolution and precipitation of carbonate and silicate mineral and cation exchange, and identification of karst hydrogeological systems including: the process of karst groundwater recharge, flow, and discharge. In addition to explaining the hydrochemical processes, the studies that apply multivariate statistics can also unfold the relationships between hydrochemical facies and aquifer groups and between the hydraulic characteristics of faults and physical-chemical processes in aquifers.

The majority of karst hydrogeological studies take place in nontropical regions in Paleozoic-Mesozoic rocks whose groundwater has varying electrical conductivity (EC) or total dissolved solids (TDS), like studies conducted by Yidana et al. (2010), (2011), Belkhiri et al. (2011), Narany et al. (2014), Chihi et al. (2015), and Yuan et al. (2017); for these studies, grouping using multivariate analysis can adequately explain hydrochemical characteristics. Karst groundwater in the tropics in Cenozoic rocks has a low variability of EC. To produce a more convincing multivariate analysis using EC of low variability, a validation that relies on stable and unstable isotopes as tracer agents becomes necessary.

The stable isotopes and ^{222}Rn have been widely applied as tracers in groundwater studies. The isotopes ^{18}O and ^{2}H are conservative (Falcone et al. 2008; Pu et al. 2013; Tillman et al. 2014; Murillo et al. 2015; and Sun et al. 2016), that is, not affected by water–rock interaction processes at temperatures lower than 200 °C (Marfia et al. 2004). These isotopes have been used in studies of groundwater recharge and flow (Marfia et al. 2004; Rodgers et al. 2005; Blasch and Bryson 2007; Mukherjee et al. 2007; Ryu et al. 2007; Al-Gamal 2011; Singh et al. 2013), the heterogeneity of aquifer hydraulic properties (Marfia et al. 2004; Leibundgut et al. 2009; Doveri et al. 2013), residence time of groundwater (Rademacher et al. 2003; Mahlknecht et al. 2006), and the mixing of groundwater from different sources (Coplen 1993). The isotope ^{222}Rn can also be used as a tracer element (Burnett et al. 2001) because, in addition to having a short half-life of 3.8 days (Michel 1990; Clark and Fritz 1997), it is a noble gas that has the highest water solubility (Clever 1985) through diffusion. Moreover, it is conservative, meaning that it does not react with the surrounding environment (Clark and Fritz 1997). The study of fractured aquifers using ^{222}Rn has successfully pinpointed areas affected by faults (Choubey and Ramola 1997; Villalobos et al. 2017) and regions with intensive fractures and active hydraulic characteristics (Cook et al. 1999; Hamada 1999; Skeppstrom 2005), to identify geological controls on water chemistry in geothermal systems (Iskandar et al. 2018), and to assist in groundwater studies in karst aquifers (Criss et al. 2007).

By conducting a validated hydrochemical study with stable isotopes and ^{222}Rn data on a more detailed scale, a thorough comprehension of hydrogeological characteristics in relation to lithological control and geological structure, as well as the origin of groundwater in the study area, can be achieved and, therefore, used as the basis for spring management. This study hypothesizes that important springs (with large discharges) have a deep groundwater system that not only interacts with carbonate rocks but also with nonkarst (siliciclastic) rocks, which are controlled by geological structures.

Geological and hydrogeological setting

The study area is an anticlinorium zone with an east–west direction, forming a range of hills at an elevation averaging less than 500 m above sea level (masl) (Bemmelen 1949). Geomorphologically, it is dominated by structural hills, karst morphology, low to undulating hills, and a small portion of volcanic cones that are geologically composed of various rock formations such as carbonate rocks, siliciclastic sediments, and volcanic rocks (Luthfi et al. 2017; Novita et al. 2017). Karst morphology develops in limestones of the Bulu Formation with isolated karst cone patterns. The spatial variation of the lithological types in the study area is presented in Fig. 1.

The stratigraphy of the study area is composed of rock formations from early Miocene to Pleistocene epoch (Luthfi et al. 2017; Novita et al. 2017). The limestone of the Tawun Formation (Nmtl), formed in the later early Miocene, is composed of sandy marl alternating with bioclastic limestone, with coarse grains at several sites. The quartz sandstone of the Ngrayong Formation (Nmns), formed in the middle Miocene, is composed of quartz sandstones with limestones and sandy limestone intercalations. The limestone of the Bulu Formation (Nmbl), formed in the later middle Miocene, is composed of layered clastic limestone (packstone-wackestone), which is solid, locally jointed, and porous. The sandstone of the Wonocolo Formation (Nmws), formed in the later middle Miocene, is composed of calcareous sandstone with sandy marl intercalations. The sandstone of the Ledok Formation (Nmls), formed in the late Miocene, is composed of glauconitic sandstones in layered structures of coarse to fine sand, and cemented by carbonates. The limestone of the Ledok Formation (Nmll), formed in the late Miocene, is composed of clastic limestone, of medium to fine sand. The marl of the Mundu Formation (Npmm), formed in the Pliocene, is distributed around the synclinal axis. The limestone of the Paciran

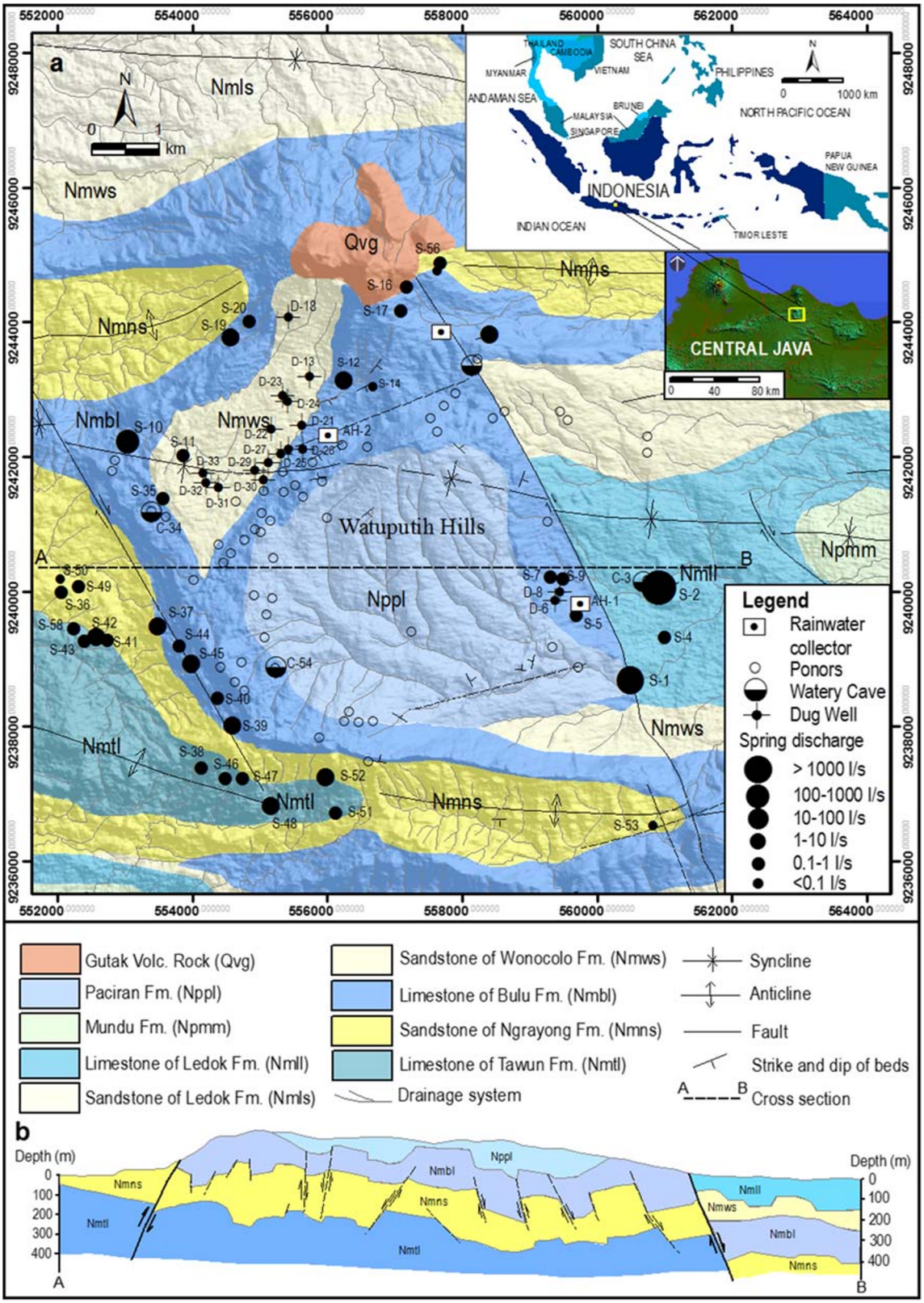

Fig. 1 **a** Map of the geology and hydrogeological sampling features in the study area (Modified from Luthfi et al. 2017; Novita et al. 2017). **b** Geological cross section along the A–B line, based on resistivity and gravity anomalies investigation (GAI, Geological Agency of Indonesia, Jakarta, Indonesia, unpublished report, 2017)

Formation (Nppl), formed in the Pliocene-Pleistocene, is composed of layered clastic limestone, with fine-to-very-coarse grain size, and is distributed in Watuputih Hills surrounded by the limestones of Bulu Formation. The Gutak Volcanic Rocks (Qvg), formed in the Pleistocene, are composed of dacitic andesitic lava, andesitic breccia, and andesitic intrusions in the northern part of the study area.

The geological structures developed in the study area are folds (syncline, anticline), with west–east and northwest–southeast directions, and northwest–southeast-oriented faults. The anticlines in the south and north and the syncline in the middle of the study area plunge to both directions. This syncline is partially covered by the limestone of the Paciran Formation. In the north, there is another syncline thrusting from the east. Meanwhile, in the east and west, there is a northwest–southeast-oriented lateral or strike-slip fault (Luthfi et al. 2017; Novita et al. 2017). Such complex geological structures are apparent in the geological cross-sections, a product of geophysical investigations conducted by the Geological Agency of Indonesia-GAI (Geological Agency of Indonesia, Jakarta, Indonesia, unpublished report, 2017) using resistivity and gravity anomalies (Fig. 1). The cross-sections also show a downthrown block in the eastern lateral fault and a slightly upthrown wall on the western lateral fault. In the middle of the study area, the fault systems cut through the limestone of the Tawun Formation, the quartz sandstone of the Ngayong Formation, and the limestone of the Bulu Formation. These faults are not visible on the surface because they are covered by the limestone of the Paciran Formation that forms Watuputih Hills.

The development of the hydrogeological system in the study area is indicated by the presence of around 39 springs and four cave streams around the limestones of the Paciran Formation (Fig. 1). Based on the results of measurements in the dry season (July–August 2017), the springs' discharge varies from 0.01 to 1,516 L/s with a geometric average of 0.5 L/s. The springs are generally permanent and, based on lithological conditions, divided into two types, namely springs in karst rocks and springs in nonkarst rocks. The typology of the former refers to the classification of karst springs (Ford and Williams 2007), which includes artesian fault-guided springs and free-draining or contact springs. The artesian fault-guided springs emerge through a fault plane and have eroded impermeable layers in the limbs of the folds. The contact springs are formed on the cliffs of a valley by gravity or due to the presence of an impermeable layer under the karst rocks (Ford and Williams 2007).

Materials and methods

Field sampling

Samples, consisting of waters from 33 springs, four cave waters, and 13 dug wells, were taken in July–August 2017 for hydrochemical and stable isotope (^{18}O and ^{2}H) analysis. Some parameters like temperature, pH, electrical conductivity (EC), HCO_3^-, and radon (^{222}Rn) were examined in the field. The temperature, EC, and pH were measured with a portable LaMotte water testing kit. Meanwhile, the HCO_3^- ion and ^{222}Rn concentration were determined using an alkalinity test kit by titration and RAD7, respectively. The stable isotope analysis of rainwater was carried out every month for 1 year (2018) at three locations to determine the local meteoric water line (LMWL) equation.

The sampled waters were filtered using a 0.45-μm syringe filter and then inserted into two 200-ml polyethylene bottles, each for anion and cation analysis. For cation analysis, the water samples were acidified with 0.1 N HNO_3 to prevent precipitation. All water samples were preserved at 4 °C for transport to the laboratory. The ^{222}Rn concentrations in the field were measured with RAD7 connected to the RAD-H_2O accessory. The water sample was poured into a 250-ml reagent bottle attached to the scintillator. Air was then circulated in a closed circuit for 5–10 min until the ^{222}Rn was mixed homogeneously with the air, and the resulted ^{222}Rn activity was recorded directly. Each sample was subjected to five measurement cycles.

Hydrochemical analysis

Analysis of major ions, namely Ca^{2+}, Na^+, Mg^{2+}, K^+, HCO_3^-, SO_4^{2-}, Cl^-, and NO_3^-, was carried out in the hydrochemical laboratory of the Center for Groundwater and Environmental Geology, the Geological Agency of Indonesia. Ions Ca^{2+}, Na^+, Mg^{2+}, and K^+ were analyzed using the Dionex ICS-1500 ion chromatography system. As for SO_4^{2-} and NO_3^-, these ions were determined with a Varian Cary 100 UV-Vis spectrophotometer. Meanwhile, Cl^- and HCO_3^- were measured with argentometric titration and alkalinity titration, respectively. The laboratory analysis results can be used only if the charge balance error (CBE) is <5% (Yidana et al. 2010, 2011, 2017; Al-Charideh 2011; Wu et al. 2013), which, in this study, was calculated using the following equation (Freeze and Cherry 1979):

$$\%\mathrm{CBE} = \frac{\sum Zm_c - \sum Zm_a}{\sum Zm_c + \sum Zm_a} \times 100 \quad (1)$$

The notation Z is ionic valence, m_c is molality of cations, and m_a is molality of anions.

Stable isotope analysis

The stable isotope analysis was performed in the hydrochemical laboratory of the Center for Groundwater and Environmental Geology, the Geological Agency of Indonesia. The $\delta^{18}O$ and $\delta^{2}H$ values were measured relative to Vienna Standard Mean Ocean Water (VSMOW) using the

Table 1 Results of physical-chemical analysis and hydrochemical facies of the water samples in the study area

No.	ID	Site name	Temp. (°C)	EC (μS/cm)	pH	Ca (mg/L)	Mg (mg/L)	K (mg/L)	Na (mg/L)	HCO_3 (mg/L)	Cl (mg/L)	SO_4 (mg/L)	NO_3 (mg/L)	Pco_2 (%)	SIc	SId	CBE (%)	Hydrochem. Facies
1	S-1	Brubulan Tahunan	27.1	521	7.20	92.7	12.5	1.5	5.1	366.1	5.8	4.4	15.2	2.3	0.28	0.07	−4.7	Ca-HCO_3
2	S-2	Sumbersemen	26.5	551	7.21	86.8	16.7	1.7	3.3	341.6	6.6	4.4	10.4	2.0	0.23	0.11	−1.3	Ca-Mg-HCO_3
3	C-3	Rambut	26.8	545	7.20	83.9	16.4	1.7	3.9	299.0	7.0	0.1	12.3	1.9	0.16	−0.02	4.1	Ca-Mg-HCO_3
4	S-4	Kalutan	26.9	606	7.11	120.0	4.2	1.5	10.2	372.2	9.7	7.6	25.7	2.8	0.30	−0.49	−1.0	Ca-HCO_3
5	S-5	Ngrojo	27.1	838	7.06	147.0	3.7	7.3	16.9	384.4	38.5	21.6	82.9	3.2	0.32	−0.58	−3.5	Ca-HCO_3
6	S-7	Ngandong	27.4	620	7.16	130.9	2.4	1.5	4.0	414.9	8.9	0.0	5.8	2.8	0.44	−0.46	−1.4	Ca-HCO_3
7	D-8	Mainah	25.8	826	7.25	147.2	7.4	12.2	21.1	457.7	36.2	25.2	24.8	2.5	0.58	0.24	−1.4	Ca-HCO_3
8	S-9	Gempol	27.4	535	7.47	99.7	5.8	1.6	10.1	329.5	13.6	4.4	0.0	1.1	0.52	0.17	0.5	Ca-HCO_3
9	S-10	Brubulan Pesucen	27.8	547	6.94	91.1	15.4	1.0	2.7	322.1	4.7	2.2	30.9	3.7	−0.03	−0.46	0.0	Ca-Mg-HCO_3
10	S-12	Sumber Suntri	26.5	549	6.99	109.6	3.5	0.5	3.2	366.0	3.9	2.8	5.4	3.7	0.14	−0.83	−2.8	Ca-HCO_3
11	D-13	Suntri	25.3	708	7.16	127.7	7.7	3.4	11.9	361.8	25.3	31.2	14.2	2.4	0.34	−0.17	0.6	Ca-HCO_3
12	S-14	Plenggong	25.8	632	7.31	114.9	6.4	1.2	3.1	311.2	8.9	4.3	32.9	1.4	0.39	−0.12	3.7	Ca-HCO_3
13	S-15	Sumber Bitingan	26.7	805	7.09	130.1	12.2	17.5	15.6	414.9	29.6	43.6	26.4	3.2	0.31	−0.05	−2.0	Ca-HCO_3
14	S-16	Klatak	25.1	214	6.73	17.6	6.1	2.9	17.4	97.6	15.6	0.3	0.0	1.9	−1.38	−2.86	4.0	Ca-Na-Mg-HCO_3-Cl
15	S-17	Bitingan	27.1	537	6.82	84.7	15.6	1.8	7.7	366.1	7.0	0.0	0.0	5.4	−0.16	−0.70	−2.6	Ca-Mg-HCO_3
16	D-18	Picisan	26.5	806	7.01	124.2	18.1	6.0	22.1	494.9	33.5	29.1	3.0	4.7	0.30	0.14	−4.9	Ca-HCO_3
17	S-19	Sumber Brengkeng1	27.1	592	7.26	103.9	11.4	2.1	7.6	396.6	7.4	19.4	2.6	2.1	0.40	0.21	−4.7	Ca-HCO_3
18	S-20	Brekngkeng	26.8	625	7.25	116.2	10.4	1.0	5.8	384.4	7.0	3.9	0.0	2.1	0.44	0.20	2.7	Ca-HCO_3
19	D-21	Sumur Dukoh	26	526	7.15	91.1	7.5	1.2	7.1	317.3	9.7	23.8	3.8	2.2	0.16	−0.39	−4.4	Ca-HCO_3
20	D-22	Cemara	27	632	7.26	98.3	16.8	1.3	11.6	341.7	19.5	50.4	18.0	1.8	0.30	0.19	−4.6	Ca-HCO_3
21	D-23	Klencong	25.8	777	7.05	116.2	19.4	18.5	16.0	439.3	29.2	60.3	0.0	3.8	0.26	0.11	−4.0	Ca-HCO_3
22	D-24	Klencong2	26	591	7.23	92.5	19.1	2.0	6.6	378.3	8.2	30.8	4.9	2.1	0.29	0.25	−4.5	Ca-Mg-HCO_3
23	D-25	Sumur Gede	27.2	698	7.17	101.3	15.6	4.7	25.6	439.3	19.5	20.4	6.5	2.9	0.33	0.20	−4.4	Ca-HCO_3
24	D-26	Sumur Agung	25.1	901	7.05	92.7	11.4	59.7	48.8	274.6	63.8	78.8	31.2	2.4	−0.03	−0.60	4.4	Ca-Na-HCO_3-Cl
25	D-27	Waru	25.3	836	6.95	153.1	10.7	5.2	18.6	476.0	22.2	15.2	0.0	5.0	0.29	−0.22	4.5	Ca-HCO_3
26	D-28	Sumber Belik	26.1	707	7.16	119.4	8.5	10.8	18.2	353.9	37.0	25.3	15.9	2.3	0.29	−0.22	0.7	Ca-HCO_3
27	D-30	Muslim	26.6	805	6.90	96.7	32.9	17.5	19.4	396.6	44.7	28.8	29.0	4.8	−0.02	−0.14	0.0	Ca-Mg-HCO_3
28	D-32	Timbrangan	28.8	453	7.28	83.9	4.5	0.5	2.5	219.7	7.8	16.8	26.9	1.1	0.11	−0.69	0.8	Ca-HCO_3
29	C-34	Menggah	26.4	607	7.26	91.1	7.9	1.8	3.3	299.0	8.6	2.1	12.0	1.6	0.25	−0.19	0.1	Ca-HCO_3
30	S-36	Tanimulya	24.9	415	6.52	42.2	7.2	27.1	17.2	79.8	51.4	44.4	14.4	2.5	−1.35	−3.10	3.3	Ca-Cl-HCO_3-SO_4
31	S-37	Kajar	25.9	551	7.18	90.0	17.6	1.2	3.0	341.7	6.6	9.3	14.3	2.3	0.24	0.16	−0.9	Ca-Mg-HCO_3
32	S-38	Sendang Sayuran	26.7	589	7.08	124.5	2.7	0.6	3.1	402.7	5.8	8.5	5.8	3.3	0.33	−0.62	−3.2	Ca-HCO_3
33	S-39	Mermo	26.2	462	7.24	85.8	7.4	0.8	2.8	292.8	5.8	2.7	10.8	1.7	0.20	−0.30	−1.5	Ca-HCO_3
34	S-40	Waru	26.1	792	7.11	114.4	32.7	7.5	6.0	476.0	13.6	27.1	7.2	3.5	0.35	0.54	0.0	Ca-Mg-HCO_3
35	S-41	Bibis	27.4	697	7.02	128.0	10.3	4.4	10.1	396.6	15.6	48.6	5.0	3.5	0.21	−0.33	−1.6	Ca-HCO_3
36	S-42	Cumpleng	28.2	681	7.02	109.6	20.0	3.7	8.5	366.1	15.2	47.7	9.8	3.4	0.13	−0.13	0.0	Ca-Mg-HCO_3
37	S-43	Aren	27.1	922	7.24	165.1	25.3	2.0	17.9	410.2	11.7	189.6	0.0	2.2	0.51	0.57	0.8	Ca-HCO_3-SO_4
38	S-44	Sumberan 2	26.2	849	7.16	108.8	42.6	6.9	8.2	482.1	21.0	52.7	9.6	3.2	0.36	0.67	−1.4	Ca-Mg-HCO_3
39	S-45	Sumberan	25.8	700	7.20	95.1	31.9	5.2	6.5	439.3	14.8	29.3	9.9	2.6	0.32	0.53	−3.7	Ca-Mg-HCO_3
40	S-47	Ngleweh	27.4	495	7.18	94.9	6.3	1.1	3.5	319.6	7.8	5.3	3.4	2.1	0.23	−0.35	−1.8	Ca-HCO_3
41	S-48	Jurangjero	27.1	579	7.23	91.1	24.0	2.8	6.7	341.7	7.8	32.3	7.1	2.0	0.27	0.35	2.1	Ca-Mg-HCO_3

Table 1 (continued)

No.	ID	Site name	Temp. (°C)	EC (µS/cm)	pH	Ca (mg/L)	Mg (mg/L)	K (mg/L)	Na (mg/L)	HCO_3 (mg/L)	Cl (mg/L)	SO_4 (mg/L)	NO_3 (mg/L)	Pco_2 (%)	SIc	SId	CBE (%)	Hydrochem. Facies
42	S-49	Jatimalang	26.5	315	6.50	33.4	2.1	31.5	16.6	36.5	46.7	40.0	24.8	1.2	−1.80	−4.43	3.8	Ca-K-Na-Cl-SO_4
43	S-51	Plumpung	26.7	765	7.21	111.4	27.7	5.4	13.5	439.3	21.8	70.1	7.8	2.6	0.38	0.52	−4.6	Ca-Mg-HCO_3
44	S-52	Duwur	26.1	601	7.16	95.1	22.8	1.3	5.2	360.0	9.3	12.1	15.1	2.4	0.21	0.17	1.7	Ca-Mg-HCO_3
45	S-53	Sami	26.8	887	7.17	155.2	24.2	1.4	12.9	530.9	11.7	53.3	0.0	3.4	0.56	0.68	1.1	Ca-HCO_3
46	C-54	Manuk	25.6	737	7.21	96.7	31.4	7.0	5.6	414.9	14.0	18.1	39.9	2.5	0.34	0.56	−2.3	Ca-Mg-HCO_3
47	S-55	Ngeso	25.5	763	7.16	113.0	30.5	1.7	11.3	549.2	5.1	18.7	2.3	3.6	0.45	0.71	−4.8	Ca-Mg-HCO_3
48	S-56	Kahuripan	26.6	503	7.25	62.3	21.2	2.0	14.1	280.7	4.7	31.9	0.4	1.5	0.04	−0.02	1.1	Ca-Mg-HCO_3
49	C-57	Temuireng	27.6	643	7.04	132.0	2.7	1.9	5.8	394.3	5.8	7.4	25.1	3.5	0.31	−0.68	−0.3	Ca-HCO_3
50	S-58	Mataair Aren2	27.8	253	6.79	36.3	4.3	3.8	6.1	115.9	11.3	8.1	3.5	1.9	−0.95	−2.46	1.9	Ca-HCO_3

Picarro L-2130-i analyzer. The allowed error in the analysis is ±0.2% for $\delta^{18}O$ or ± 1.0% for $\delta^{2}H$. The LMWL equation was determined by considering the amount-weighted factor, i.e., monthly rainfall at each rainwater sampling location, which was calculated using the following equation (Zuppi 1981; Clark 2015):

$$\delta_w = \frac{\sum_{i=1}^{n} P_i^m \delta_i^m}{\sum_{i=1}^{n} P_i^m} \quad (2)$$

The notation P_i^m represents monthly rainfall (mm) and δ_i^m is the oxygen and hydrogen isotope ratios (‰ expressed as $\delta^{18}O$ and $\delta^{2}H$).

Calculation of saturation index and partial pressure of CO_2

The saturation index for minerals (SI) and partial pressure of CO_2 (Pco_2) are parameters that determine the characteristics of a karst aquifer system (White 2015). Pco_2 serves as the basis for evaluating the level of interaction between water and CO_2, which can be calculated using the following equation (Ford and Williams 2007):

$$Pco_2 = \frac{\left(HCO_3^-\right)\left(H^+\right)}{K_1 K_{CO_2}} \quad (3)$$

The notation (HCO_3^-) is bicarbonate ions, (H^+) is hydrogen ion activity, K_1 is equilibrium constants of reactions at 25 °C, and Kco_2 is equilibrium constants for CO_2 in water at 25 °C.

The mineral saturation index (SI) can determine the degree of chemical equilibrium between water and minerals in aquifers (Domenico and Schwartz 1990; Ford and Williams 1989, 2007; Yuan et al. 2017), which, in this study, was calculated using the equation below:

$$SI = \log IAP/K \quad (4)$$

The notation K is the equilibrium constant of the mineral and IAP is the ion activity product of the mineral. SI > 0 means that water is saturated with minerals, whereas SI < 0 signifies the opposite, i.e., water is not saturated with minerals. When SI = 0, it indicates an equilibrium water–rock interaction. This study calculated the saturation index of calcite ($CaCO_3$; expressed as SIc) and dolomite ($CaMg(CO_3)_2$; expressed as SId). The SIc and SId values generally have an error of ±0.1–0.2 (Ford and Williams 1989, 2007). The mineral saturation and Pco_2 values were calculated using the program PHREEQC (Parkhust and Appelo 1999).

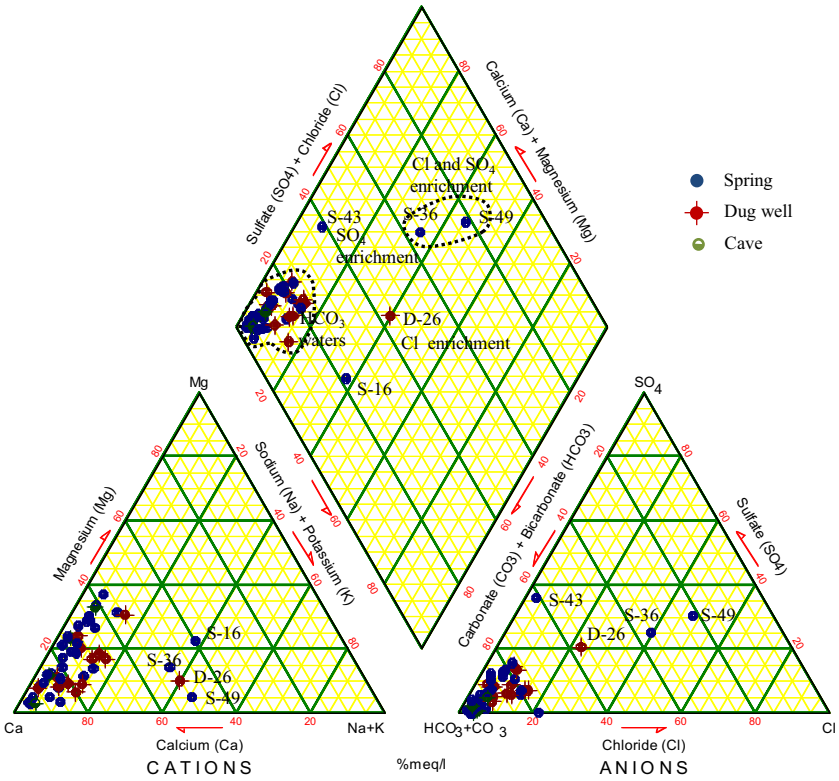

Fig. 2 Piper plot of the major ion chemistry representing the hydrochemical facies

Hierarchical clustering of hydrochemical data

Hierarchical cluster analysis is a multivariate statistical method that has been widely used in Earth sciences (Davis 1986), one of which is for hydrochemical studies (Swanson et al. 2001; Guler et al. 2002; Guler and Thyne 2004). This method has provided various benefits to explaining hydrological processes in nature (Yidana et al. 2010, 2011; Narany et al. 2014; Chihi et al. 2015; Yuan et al. 2017). This technique is useful for pinpointing similarity and dissimilarity in a group of data based on the Euclidean distance; the smaller the distance, the more similar the data group is (Yidana et al. 2010, 2011). The Euclidean distances are calculated, preferably, using parameters with the highest variant, instead of those with the lowest one (Guler et al. 2002). Parameters with the most similarity are grouped into one cluster and then linked to another cluster based on this similarity; therefore, clusters connected with shorter relationship distances share more similarities to each other than those with longer ones (Yidana et al. 2010, 2011). For this analysis, the required data included temperature, EC, pH, Ca^{2+}, Mg^{2+}, Na^{+}, K^{+}, HCO_3^{-}, SO_4^{2-}, Cl^{-}, Pco_2, SIc, and SId. Major cations such as Ca^{2+}, Mg^{2+}, and HCO_3^{-} are autochthonous as the results of the dissolution of limestone, whereas the anions Cl, Na, K, SO_4 are allochthonous (Valdes et al. 2007). This analysis was performed in SPSS Statistics v20.

Results

Hydrochemical characteristics

For the hydrochemistry and environmental isotopes in the study area, the water samples were divided into three types, namely spring (S), dug well (D), and cave water (C). The analysis results of major ions and groundwater type, according to the Szczukariew-Priklonski's hydrochemical classification scheme (Jankowski 2001), are summarized in Table 1 and graphically depicted in a Piper diagram in Fig. 2. The order of cation abundance from the highest to the lowest is Ca^{2+} (average = 102.99 mg/L), Mg^{2+} (14.50 mg/L), Na^{+} (10.67 mg/L), and K^{+} (6.16 mg/L), while the order of the anion abundance is HCO_3^{-} (average = 357.75 mg/L), SO_4^{2-} (26.29 mg/L), and Cl^{-} (16.93 mg/L). The Piper diagram shows that the groundwater samples are dominantly bicarbonate types, and some of them indicate enrichment of Cl (D-26), SO_4 (S-43), and both Cl and SO_4 ions (S-49 and S-36).

The hierarchical group analysis based on the Euclidean distance is presented in a dendrogram (Fig. 3). For the Euclidean distance of 5, the water samples are divided into four hierarchical groups, namely group one (C1; 25 samples), group two (C2; 19 samples), group three (C3; two samples), and group four (C4; four samples; Table 2). Electrical conductivity (EC) is the most crucial factor that distinguishes one

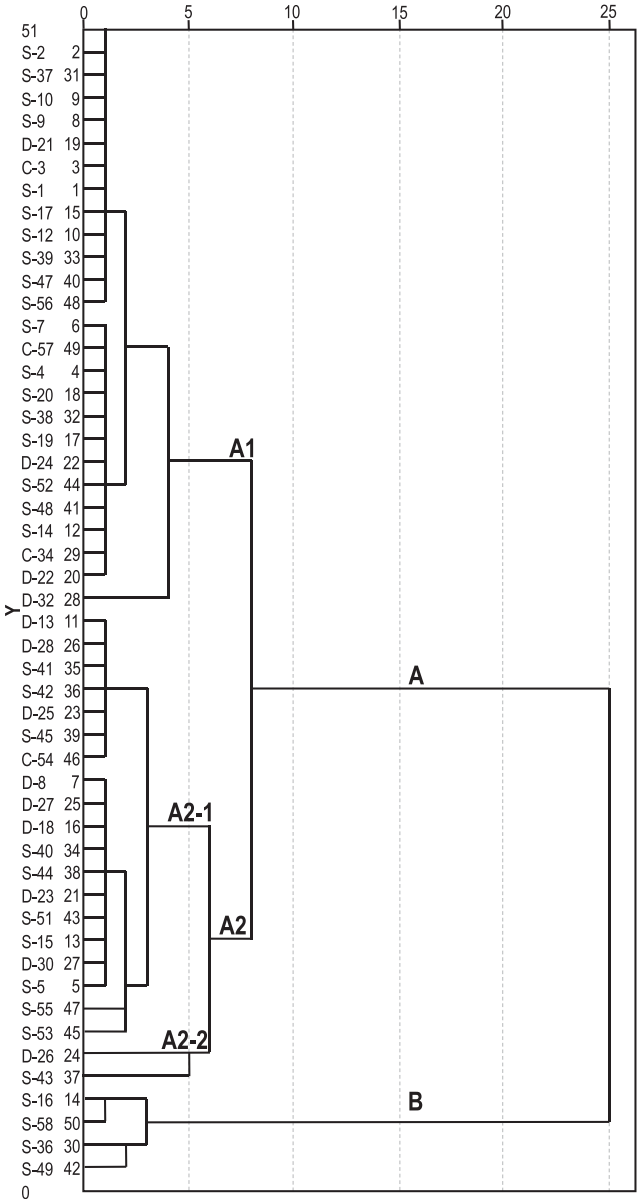

Fig. 3 Dendrogram of water samples grouping based on hierarchical cluster analysis

group from another. The EC and major ions composition in group C1 are lower than in C2. Group C4 has lower EC, pH, and compositions of Ca^{2+}, Mg^{2+}, HCO_3^- than $C1^-$ and C2. Since group C3 is characteristically similar to C2, the discussion is focused on three main groups, namely C1, C2, and C4. Based on the hierarchical division, the intensive mineral dissolution is the highest in water samples included in groups C2 and C3, then followed by group C1 and, the lowest, group C4.

Group C1 is mainly scattered in the geological structure zone (faults, folds) and the contact between limestones and two types of rocks, namely calcareous sandstones and quartz sandstones (Fig. 4). The groundwater in group C1 has types Ca-HCO_3 (64%) and Ca-Mg-HCO_3 (36%), most of which comes from springs that are controlled by the underlying geological structure (artesian fault-guided spring) and cave waters, and some are from contact springs and dug wells. Springs with large discharge are included in this group, for instance, Sumbersemen (S2), Brubulan Tahunan (S1), and Brubulan Pesucen (S10) with instantaneous discharges of 1,516, 165, and 95 L/s., respectively. Group C2 is spread mainly in layered limestones, calcareous sandstones, fault zones, and the places of contact between limestones and quartz sandstones. The groundwater in this group has types Ca-HCO_3 (58%) and Ca-Mg-HCO_3 (42%), most of which comes from dug wells and contact springs, and some are from springs in the fault zone and one cave water. The groundwater in group C3 has types Ca-Na-HCO_3-Cl and Ca-HCO_3-SO_4, which is found in calcareous sandstones (dug wells) and the sites of contact between limestones and quartz sandstones (contact springs). Group C4 has varied groundwater types, namely Ca-HCO_3, Ca-Na-Mg-HCO_3-Cl, Ca-Cl-HCO_3-SO_4, and Ca-K-Na-Cl-SO_4. These groundwater types come from nonkarst springs, namely three springs in quartz sandstones and one spring in volcanic rocks.

The study area is primarily composed of carbonate rocks. Accordingly, one of the important hydrochemical processes is chemical weathering, which refers to a chemical reaction between water and the constituent minerals of rocks at low temperatures (Kehew 2001). The Mg^{2+}/Ca^{2+} ratio reflects the intensity of carbonate rock dissolution. The ratio for dolomite dissolution is approximately 1 (El-Fiky 2010), while 0.5–1 indicates calcite dissolution (Mayo and Loucks 1995; Rajmohan and Elango 2004). The Mg^{2+} vs. Ca^{2+} plots show that most of the groundwater samples are below the line $Mg^{2+}/Ca^{2+} = 0.5$ or $Mg^{2+}/Ca^{2+} < 0.5$ (Fig. 5), indicating the effects of silicate dissolution along with the dominant calcite dissolution (Narany et al. 2014; Katz et al. 1997; Thilakerathne et al. 2015). The Mg^{2+}/Ca^{2+}ratios range from 0.03 to 0.56 (average = 0.20) in group C1, 0.04–0.65 (average = 0.30) in C2, 0.20 and 0.25 in group C3, and 0.10–0.57 (average = 0.29) in group C4. The Mg^{2+}/Ca^{2+}ratios of the water samples in the study area are mainly in the range of 0.1–0.33, and the enrichment of Ca^{2+} and Mg^{2+} ions in group C2 implies greater water-carbonate rock interaction.

The interaction between water and carbonate rocks is the primary determinant in the hydrochemistry of karst aquifers. Such interaction is expressed as the saturation index for dolomite (SId) and calcite (SIc; Fig. 6). Most of the water samples in group C1 are saturated with calcite (SIc = −0.16–0.52, average = 0.24) but not with dolomite (SId = −0.7–0.35, average = −0.18). The majority of water samples in group C2 are saturated both with calcite (SIc = 0.02–0.58, average = 0.32) and dolomite (SId = −0.58–0.71, average = 0.16). In group C3, the values of the SIc are −0.03 and 0.51, while the values of the SId are −0.60 and 0.57. In group C4, all

Table 2 Statistical summary of the chemical-physical properties of water samples based on hierarchical cluster analysis. Averages shown in italic. Min. minimum, Max. maximum, Ave. average

Clusters	ID	Values	Temp. (°C)	EC (μS/cm)	pH	Ca (mg/L)	Mg (mg/L)	K (mg/L)	Na (mg/L)	HCO_3 (mg/L)	Cl (mg/L)	SO_4 (mg/L)	Pco_2 (mg/L)	SIc	SId
A1 (C1)	S-2, S-37, S-10, S-9, D-21, C-3, S-1, S-17, S-12, S-39, S-47, S-56, S-7, C-57, S-4, S-20, S-38, S-19, D-24, S-52, S-48, S-14, C-34, D-22, D-32	Min.	25.8	453	6.82	62.3	2.4	0.5	2.5	219.7	3.9	0.0	1.1	−0.16	−0.83
		Max.	28.8	643	7.47	132.0	24.1	2.8	14.1	414.9	19.5	50.4	5.4	0.52	0.35
		Ave.	*26.8*	*563.7*	*7.18*	*98.7*	*11.2*	*1.4*	*5.7*	*342.4*	*7.9*	*11.5*	*2.4*	*0.24*	*−0.18*
A2–1 (C2)	D-13, D-28, S-41, S-42, D-25, S-45, C-54, D-8, D-27, D-18, S-40, S-44, D-23, S-51, S-15, D-30, S-5, S-55, S-53	Min.	25.3	681	6.90	95.1	3.7	1.4	5.6	353.9	5.1	15.2	2.3	−0.02	−0.58
		Max.	28.2	887	7.25	155.2	42.7	18.5	25.6	549.2	44.7	70.1	5.0	0.58	0.71
		Ave.	*26.4*	*772.5*	*7.11*	*120.8*	*20.4*	*7.7*	*14.1*	*437.6*	*23.6*	*35.1*	*3.3*	*0.32*	*0.16*
A2–2 (C3)	D-26, S-43	Min.	25.1	901	7.05	92.7	11.4	2.0	17.9	274.6	11.7	78.8	2.2	−0.03	−0.60
		Max.	27.1	922	7.24	165.1	25.3	59.7	48.8	410.2	63.8	189.6	2.4	0.51	0.57
B (C4)	S-16, S-58, S-36, S-49	Min.	24.9	214	6.50	17.6	2.1	2.9	6.1	36.5	11.3	0.3	1.2	−1.80	−4.43
		Max.	27.8	415	6.79	42.2	7.2	31.5	17.4	115.9	51.4	44.4	2.5	−0.95	−2.46
		Ave.	*26.1*	*299.3*	*6.64*	*32.4*	*4.9*	*16.3*	*14.4*	*82.5*	*31.2*	*23.2*	*1.9*	*−1.37*	*−3.21*

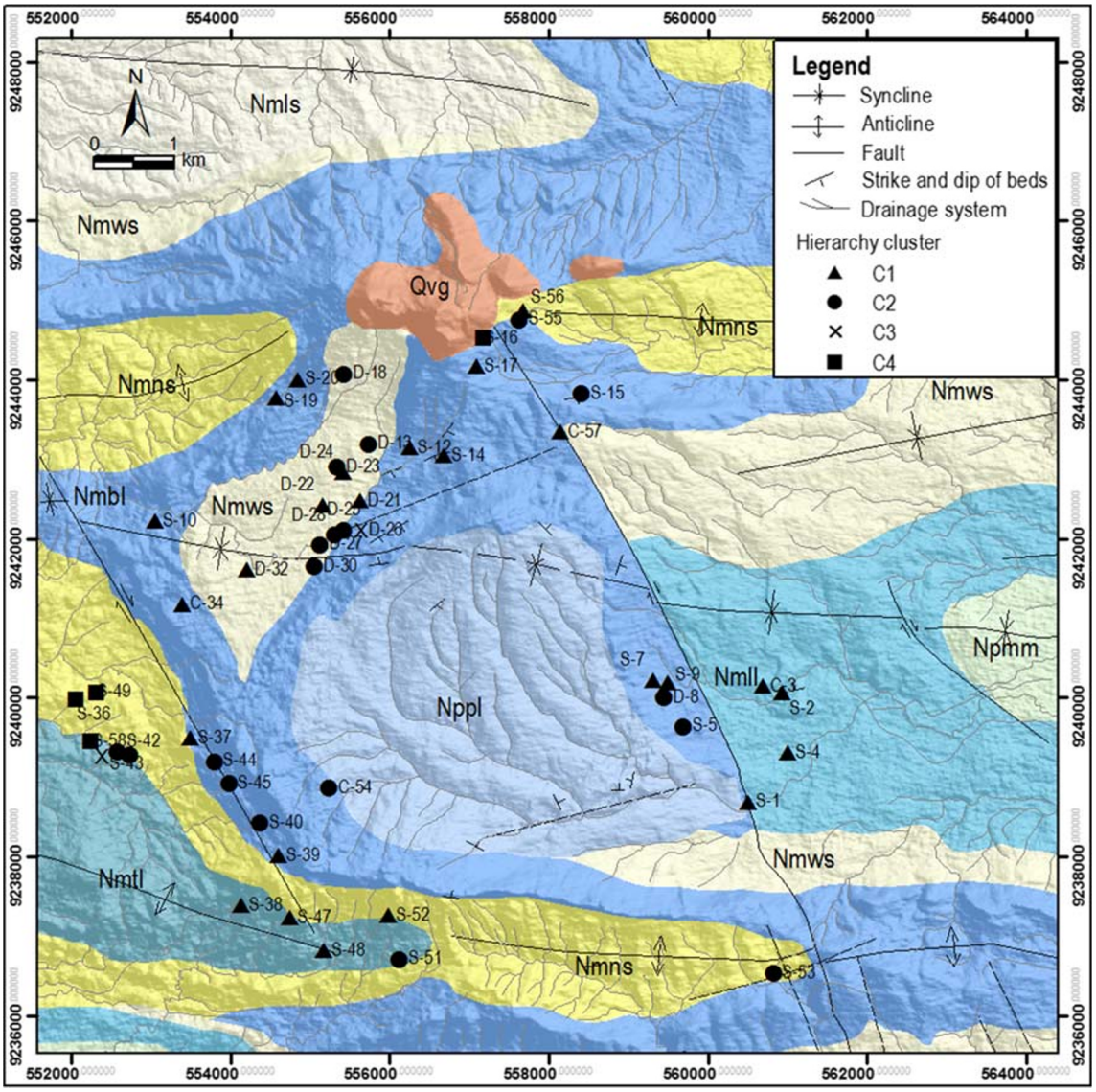

Fig. 4 Spatial distribution of water samples based on the hierarchical clustering analysis

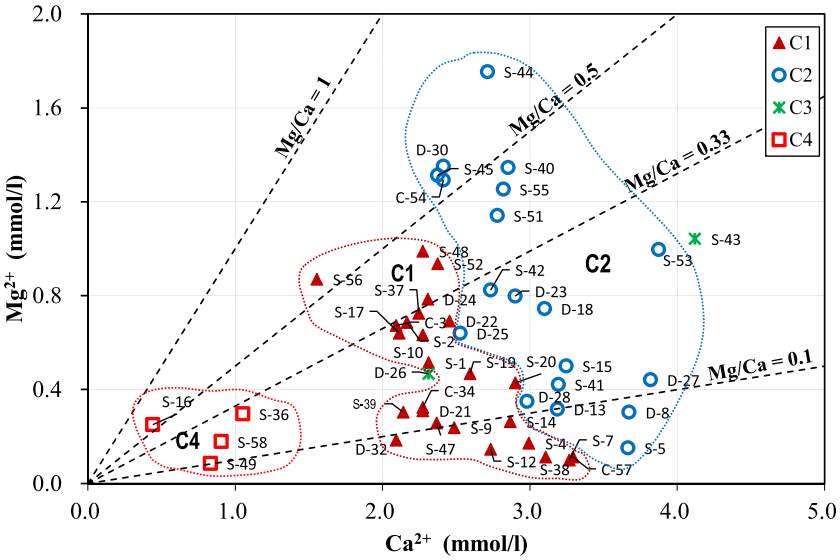

Fig. 5 Plots of Mg^{2+} versus Ca^{2+} showing that the water samples are mainly in the Mg/Ca ratios of 0.1–0.33 and also showing the enrichment of Ca^{2+} and Mg^{2+} ions in group C2

water samples are not saturated with either calcite (SIc = −1.80 to −0.95, average = −1.37) or dolomite (SId = −4.43 to −2.46, average = −3.21). With this distribution of index scores, group C2 has relatively more intensive groundwater–carbonate rock interaction (longer residence time) than group C1.

The interaction between CO_2 and water is observable by comparing Pco_2 with atmospheric conditions, which is around 0.04% (Clark 2015). The Pco_2-pH plots show that all water samples are supersaturated with CO_2 in atmospheric conditions, meaning that the groundwater has experienced CO_2 diffusion in the soil zone (Fig. 7). The Pco_2 ranges from 1.07 to 5.37% (average = 2.37%) in group C1, 2.34–4.68% (average = 3.33%) in group C2, 2.24 and 2.40% in group C3, and 1.2–2.45% (average = 1.88%) in group C4. The analysis results revealed that the water samples in group C2 had the highest Pco_2 and, therefore, the most intensive CO_2-H_2O interaction among the groups. A high Pco_2 also indicates that the groundwater comes from an aquifer system located close to the epikarst zone (Savoy 2007).

In addition to chemical dissolution, cation exchange is also an important process in hydrochemical evolution (Charfi et al. 2013). The process is demonstrated by the decrease in Ca^{2+} and Mg^{2+} levels and the enrichment of Na^{+} ions (Schoeller 1977; Hem 1992). The cation exchange process in water samples is represented by the decrease in Ca^{2+}/Na^{+} molar ratio along with the increase in salinity (Cl^{-}; Fig. 8). This pattern was identified in three samples of springs appearing in quartz sandstones (group C4) with very strong correlations ($R^2 = 0.96$). Group C2 has a moderate correlation ($R^2 = 0.43$), while group C1

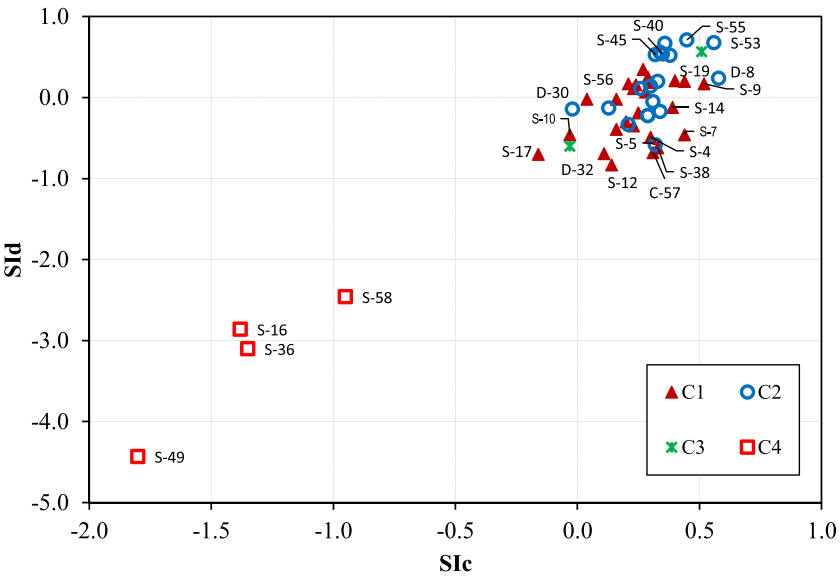

Fig. 6 Plots of the saturation index for dolomite (SId) versus calcite (SIc) showing that the most of water samples in group C2 are saturated both with calcite and dolomite

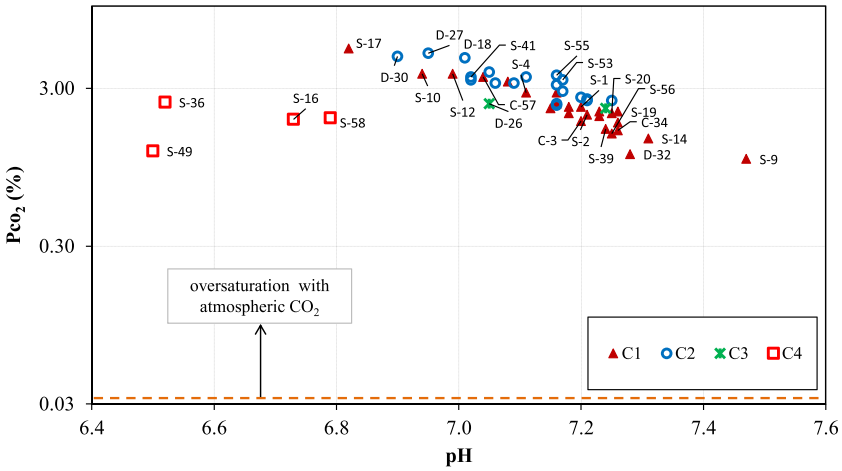

Fig. 7 Plots of Pco_2 versus pH showing that all water samples are supersaturated with CO_2 in atmospheric conditions. The water samples in group C2 had the highest average values of Pco_2

has a low correlation ($R^2 = 0.17$). Based on the Ca^{2+}/Na^+ vs. Cl^- graph, the process of cation exchange between Ca^{2+} and Na^+ occurs mainly in group C4 and less intensive in group C2. Cation exchange, i.e., the exchange of Ca^{2+} and Mg^{2+} ions by Na^+, is a common process in natural groundwater systems. It involves the potential absorption of Ca^{2+}-rich water by the surface of clay minerals and the release of Na^+, causing an increase in Na^+ concentration in groundwater (Kehew 2001).

Stable isotope characteristics

The results of the stable isotope analysis are summarized in Table 3, while the numerical ranges, averages, standard deviations (SD), and coefficient of variance (CV) based on the type of hydrogeological sampling source (caves, springs and wells) are listed in Table 4. The stable isotope composition of the samples of cave water and artesian fault-guided spring water has low standard deviation and coefficient of variance, while the composition of samples from contact springs, nonkarst springs, and dug wells has low to high standard deviation and a high coefficient of variance. These findings show that the range of the stable isotope composition in artesian fault-guided springs and cave water is relatively more homogeneous than the other water sources.

The stable isotope analysis of the local meteoric water was carried out during 1 year (2018) at three locations, and the results are presented in Table 5. The amount-weighted annual isotopic values (Table 6) were calculated by considering the intensity of the precipitation (I). The analysis of the stable isotope composition in rainwater produced a local meteoric water line (LMWL) equation $\delta^2H = 7.45\delta^{18}O + 6.45$.

The origin of groundwater can be determined by plotting its $\delta^{18}O$ and δ^2H values relative to the Global

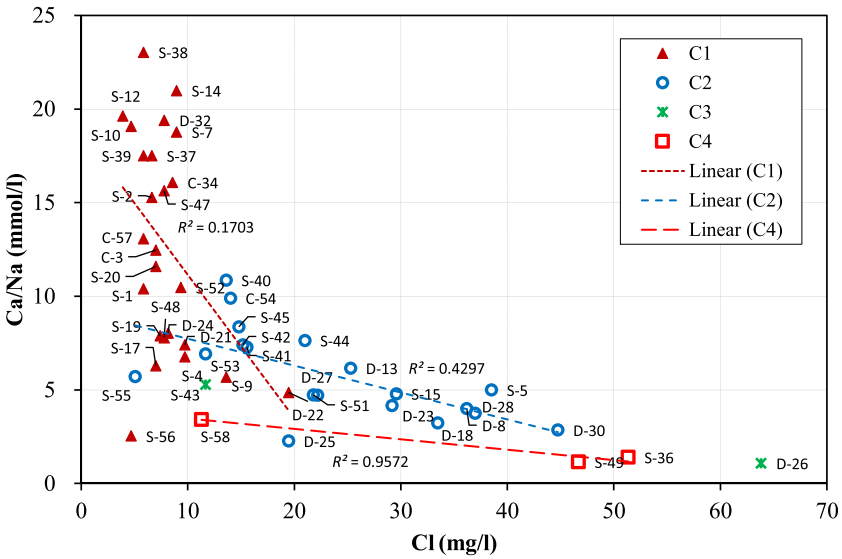

Fig. 8 Plots of Ca^{2+}/Na^+ versus Cl^- showing the very strong correlation ($R^2 = 0.96$) for the group C4, moderate correlation ($R^2 = 0.43$) for the group C2, and low correlation ($R^2 = 0.17$) for the group C1

Table 3 Results of $\delta^{18}O$ and $\delta^{2}H$ analysis and deuterium excess values of the water samples in the study area

ID	$\delta^{18}O$ (‰)	$\delta^{2}H$ (‰)	d-excess (‰)	Hydrogeological feature/type
S-1	−6.30	−40.79	9.60	Artesian fault-guided spring
S-2	−6.38	−38.89	12.17	Artesian fault-guided spring
C-3	−6.31	−38.42	12.06	Cave water
S-4	−5.82	−37.36	9.17	Artesian fault-guided spring
S-5	−6.31	−39.25	11.23	Contact spring
S-7	−6.28	−39.24	11.01	Contact spring
D-8	−6.31	−38.79	11.72	Dug well
S-9	−5.54	−34.43	9.89	Contact spring
S-10	−6.10	−37.99	10.80	Artesian fault-guided spring
S-12	−6.25	−41.04	8.93	Contact spring
D-13	−5.95	−37.83	9.76	Dug well
S-14	−6.07	−38.37	10.16	Contact spring
S-15	−6.07	−38.06	10.52	Contact spring
S-16	−6.50	−38.69	13.32	Nonkarst spring
S-17	−6.41	−39.60	11.71	Contact spring
D-18	−6.22	−37.70	12.09	Dug well
S-19	−5.54	−34.59	9.74	Contact spring
S-20	−6.06	−37.26	11.23	Contact spring
D-21	−4.96	−31.77	7.87	Dug well
D-22	−5.83	−36.55	10.10	Dug well
D-23	−5.75	−35.66	10.35	Dug well
D-24	−5.54	−33.87	10.41	Dug well
D-25	−4.43	−30.28	5.12	Dug well
D-26	−6.10	−37.31	11.46	Dug well
D-27	−4.99	−31.92	8.03	Dug well
D-28	−5.61	−35.17	9.69	Dug well
D-30	−5.82	−35.90	10.63	Dug well
D-32	−5.57	−35.50	9.02	Dug well
C-34	−6.49	−40.93	11.02	Cave water
S-36	−5.39	−35.31	7.81	Nonkarst spring
S-37	−6.40	−38.12	13.04	Artesian fault-guided spring
S-38	−6.19	−37.99	11.56	Artesian fault-guided spring
S-39	−6.33	−38.55	12.09	Artesian fault-guided spring
S-40	−6.17	−37.50	11.86	Artesian fault-guided spring
S-41	−5.93	−35.86	11.59	Contact spring
S-42	−5.84	−35.48	11.27	Contact spring
S-43	−5.59	−33.45	11.30	Contact spring
S-44	−6.06	−36.80	11.68	Artesian fault-guided spring
S-45	−6.20	−38.08	11.55	Artesian fault-guided spring
S-47	−6.28	−38.69	11.54	Artesian fault-guided spring
S-48	−6.08	−37.49	11.11	Artesian fault-guided spring
S-49	−5.98	−36.65	11.19	Nonkarst spring
S-51	−5.70	−34.88	10.70	Contact spring
S-52	−6.21	−38.03	11.63	Contact spring
S-53	−6.27	−37.78	12.34	Artesian fault-guided spring
C-54	−6.21	−37.87	11.79	Cave water
S-55	−5.93	−36.65	10.81	Contact spring
S-56	−6.26	−38.18	11.90	Contact spring
C-57	−6.40	−40.43	10.74	Cave water
S-58	−6.10	−37.70	11.09	Nonkarst Spring

Meteoric Water Line (GMWL) and the LMWL. The equation of GMWL is $\delta^{2}H = 8\delta^{18}O + 10$ (Craig 1961). The plots of the $\delta^{2}H$ and $\delta^{18}O$ values in the water samples and their association with LMWL and GMWL are presented in Fig. 9. These plots show the relative positions of the groundwater samples relative to GMWL and LMWL, which indicates that they come from modern rainwater (Li et al. 2013; Fig. 9). Most groundwater samples from the dug wells and contact springs, as well as some samples from the artesian fault-guided springs, are closer to the LMWL. Deviations from this line represent the effect of evaporation, as seen in some dug wells and one nonkarst spring, e.g., D-21, D-25, D-27, D-32, and S-36. Evaporation can occur during the process of rainwater infiltration into groundwater (Gibson et al. 2008; Li et al. 2013). The majority of the samples from artesian fault-guided springs and cave waters, and some contact springs and dug wells, have a lower isotopic composition

Table 4 Range, average, standard deviation, and coefficient of variance of the $\delta^{18}O$ and $\delta^{2}H$ values of the water samples in the study area

Hydrogeological feature/type	*N*	$\delta^{18}O$ (‰)				$\delta^{2}H$ (‰)			
		Range	Average	SD	CV	Range	Average	SD	CV
Cave waters	4	−6.5 to −6.21	−6.35	0.12	−1.93	−40.93 to −37.87	−39.41	1.50	−3.79
Artesian fault-guided springs	13	−6.40 to −5,82	−6.20	0.16	−2.56	−40.79 to −36.80	−38.16	0.98	−2.56
Contact springs	16	−6.41 to −5.54	−6.00	0.29	−4.79	−41.04 to −33.45	−37.15	2.18	−5.88
Nonkarst springs	4	−6.50 to −5.40	−5.99	0.46	−7.67	−38.69 to −35.31	−37.09	1.45	−3.91
Dug wells	13	−6.31 to −4.43	−5.62	0.54	−9.68	−38.79 to −30.28	−35.25	2.61	−7.40

with a relative position above the LMWL, signifying the nonexistence of the secondary evaporation process.

The effect of evaporation is also observable from the deuterium excess (d-excess), which can be calculated using the formula $d = \delta D - 8\ \delta^{18}O$ (Dansgaard 1964; Gat 1980). The d-excess is useful for inferring any secondary processes that shape the composition of atmospheric vapor in the evaporation-condensation cycle in nature (Craig 1961; Merlivat and Jouzel 1979; Gat et al. 1994; Machavaram and Krishnamurthy 1995). These processes affect the $\delta^{18}O$ and $\delta^{2}H$ values in groundwater (Dansgaard 1964). If the d-excess is lower than 10, that suggests that this isotopic composition is generally attributable to a secondary evaporation process (Dansgaard 1964). The d-excess values of the water samples of the artesian fault-guided springs and cave waters are >10, whereas in some contact springs, nonkarst springs, and most dug wells, these values are <10 (Table 7).

The high d-excess values in cave waters and artesian fault-guided springs and their relative positions above the LMWL indicate that during the recharge process, the rainwater is relatively less subjected to secondary evaporation. This condition suggests that the relatively deep groundwater flow system has a recharge area with lower temperature and higher relative humidity than the study area, as well as a relatively fast infiltration process (Harvey 2001; Gibson et al. 2008; Li et al. 2013). Values of d-excess in contact springs and nonkarst springs vary, with an average approaching 10. In other words, there is no consistent evidence for the secondary evaporation process, except at some locations. It also represents a relatively fast infiltration process. The average d-excess values of the dug wells are <10, indicating that the water receives supply from local rainwater, and some of the water sources such as D-21, D-25, D-27, and S-36, are affected by a secondary evaporation process during infiltration. However, some dug wells such as D-8, D-18, and D-26, and contact springs have high d-excess values, and the waters thereby originate from a

Table 5 Results of stable isotope analysis of rainwater during one year (2018) of observation. *I* rainfall intensity

Month (2018)	Location AH-1			Location AH-2			Location AH-3		
	I (mm)	$\delta^{18}O$ (‰)	$\delta^{2}H$ ($^{o}/_{oo}$)	*I* (mm)	$\delta^{18}O$ (‰)	$\delta^{2}H$ (‰)	*I* (mm)	$\delta^{18}O$ (‰)	$\delta^{2}H$ (‰)
Jan.	441.18	−8.43	−58.91	407.44	−7.99	−55.96	434.81	−8.35	−57.82
Feb.	137.51	−4.45	−23.88	169.02	−4.86	−27.41	192.90	−5.17	−30.64
Mar.	253.06	−7.01	−45.42	245.10	−7.41	−47.12	381.97	−8.00	−52.42
Apr.	178.25	−4.30	−23.26	135.28	−4.18	−21.99	60.48	−3.91	−24.44
May	41.38	−3.14	−13.80	17.19	−2.63	−7.12	48.38	−3.29	−15.08
Jun.	234.59	−5.72	−38.30	166.48	−4.83	−29.23	239.37	−5.78	−37.44
Jul.	24.19	−2.91	−18.91	14.48	−3.68	−24.20	11.14	−4.04	−27.04
Aug.	–	–	–	–	–	–	3.82	−344	−19.36
Sep.	11.46	−2.07	−5.93	9.23	−2.15	−6.92	6.68	−1.86	−5.01
Nov.	57.30	−1.55	−3.71	66.85	−3.19	−14.62	38.20	−1.64	−4.39
Dec.	206.90	−5.03	−28.96	229.18	−3.96	−23.76	237.14	−5.28	−30.49
Average	158.58	−4.46	−26.11	146.02	−4.49	−25.83	150.44	−4.61	−27.65

Table 6 Results of the amount-weighted annual analysis of rainwater stable isotope

Location ID	Location, X (m)	Location, Y (m)	Elevation (masl)	$\delta^{18}O$ (‰)	$\delta^{2}H$ (‰)
AH-1	559,739	9,239,815	180	−6.03	−38.59
AH-2	556,009	9,242,309	310	−5.82	−36.83
AH-3	557,680	9,243,842	400	−6.55	−42.33

deeper groundwater system. The same case applies to artesian fault-guided springs and cave waters.

Radon characteristics

Monitoring of the 51 hydrogeological features (caves, springs and wells) produced a range of ^{222}Rn concentrations from 441 to 19,300 Bq/m^3 with an arithmetic average of 10,322 Bq/m^3, a standard deviation (SD) of 5,038.85 Bq/m^3, and coefficient of variance (CV) of 48.82. Based on the classification of radon concentration proposed by Przylibski (2005), these water sources fall into the categories of radon-poor water to low-radon water. The spatial distribution and the measurement results of ^{222}Rn concentrations based on the geological characteristics of the hydrogeological features (caves, springs, wells) can be seen in Fig. 10 and Table 8.

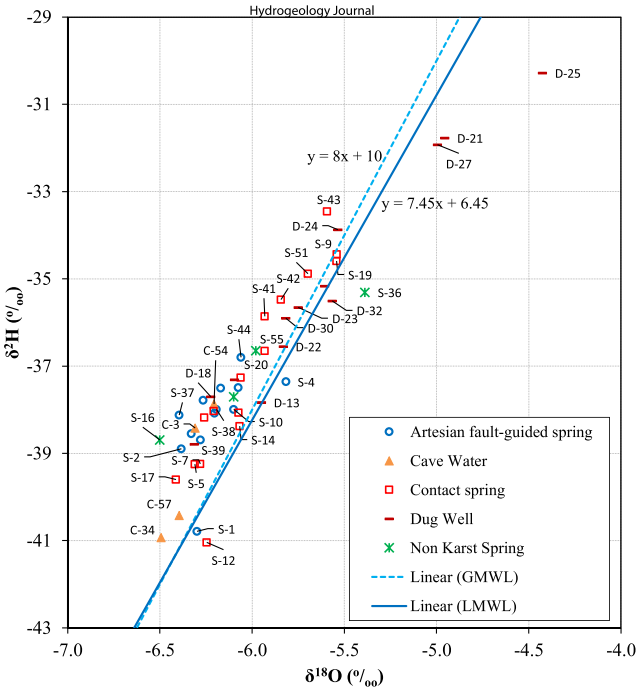

Fig. 9 Plots of $\delta^{2}H$ versus $\delta^{18}O$ values of water samples associated with the Global Meteoric Water Line (GMWL) and local meteoric water line (LMWL) in the study area

Table 7 Results of deuterium excess (d-excess) analysis of the water samples for each of the hydrogeological features. SD = standard deviation, CV = coefficient of variance

Hydrogeological feature/type	d-excess			
	Range (‰)	Average (‰)	SD	CV
Cave waters	10.7–12.1	11.4	0.6	5.4
Artesian fault-guided springs	9.2–13.0	11.4	1.1	9.3
Contact springs	8.9–11.9	10.9	0.8	7.6
Nonkarst springs	7.8–13.3	10.9	2.3	21.0
Dug wells	5.1–12.1	9.7	1.9	19.4

The ^{222}Rn concentration in the quartz sandstones of Ngrayong Formation has a relatively high value, i.e., an average 13,563 Bq/m^3 (CV = 31.31; Table 8). The high ^{222}Rn concentrations are also distributed in artesian fault-guided springs (average = 11,851 Bq/m^3; CV = 41.95), springs in the contact zone of the quartz sandstones of Ngrayong Formation (average = 11,694 Bq/m^3; CV = 19.39), and in cave waters (average = 10,315 Bq/m^3; CV = 76.10). The ^{222}Rn concentrations in dug wells average at 9367 Bq/m^3 (CV = 60.25). In the contact springs appearing in the limestones of Bulu Formation, the ^{222}Rn concentrations vary with an average of 7,521 Bq/m^3 (CV = 50.86). One spring emerging from volcanic rocks has a low ^{222}Rn concentration, that is, 1,470 Bq/m^3.

The ^{222}Rn concentration ranges in the different types of hydrogeological feature indicate correlation with lithology and geological structure. The high ^{222}Rn levels in springs emerging from the quartz sandstones of Ngrayong Formation and the sites of contact between limestones and quartz sandstones suggest that the quartz sandstone naturally has a relatively high ^{222}Rn concentration. In the springs and dug wells with the lithology of limestone and calcareous sandstones, the levels of ^{222}Rn tend to be high around the faults or folds. This finding is in line with Skeppstrom (2005), Kendall and McDonnell (1998), and Cook et al. (1999), who state that high radon concentrations are caused by rock types and rock permeability factors such as grain size and fracture intensity.

Discussion

Hydrochemical analysis that has been validated with environmental isotope data can provide a clear overview of the

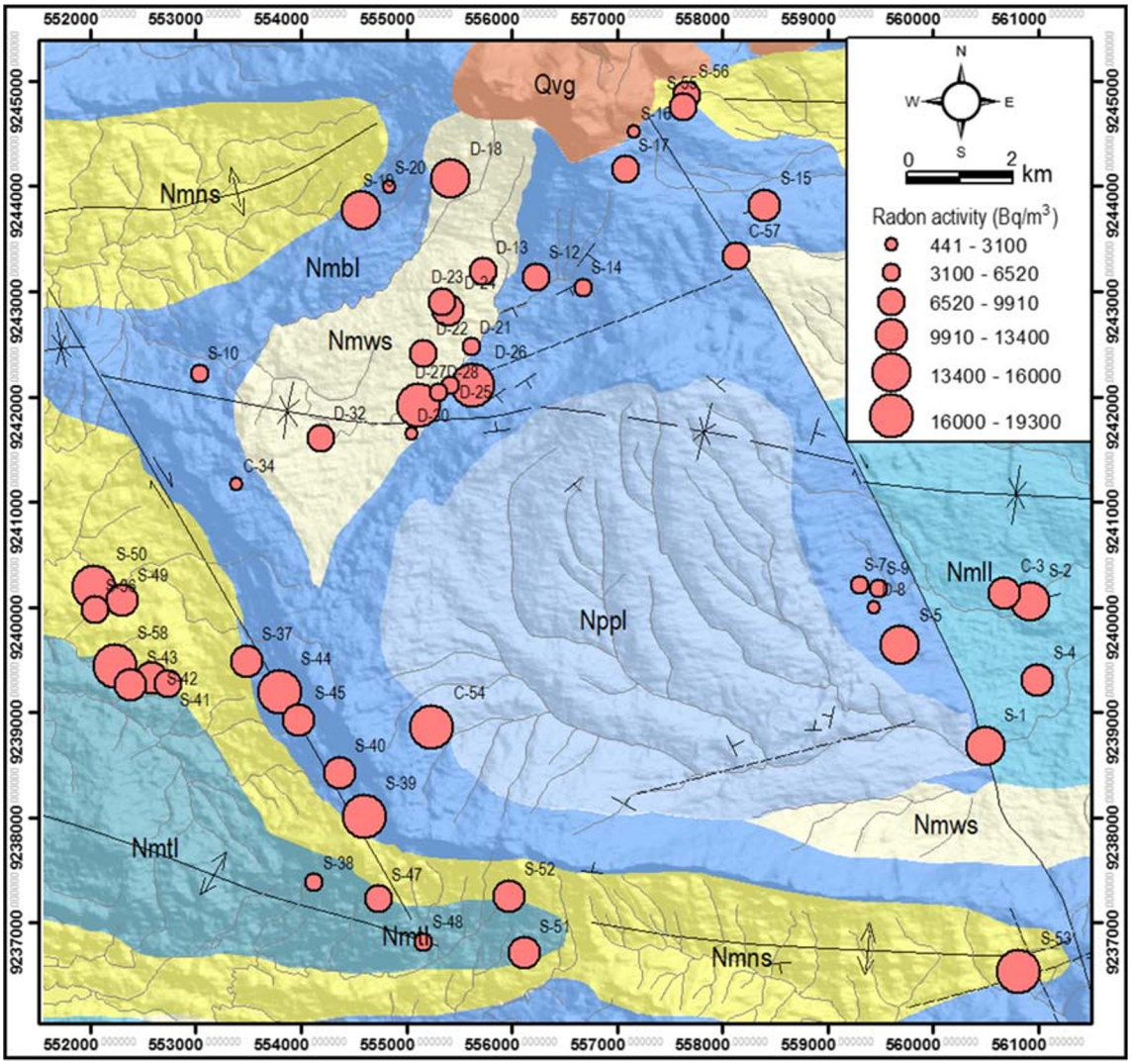

Fig. 10 Spatial distribution and classes of ^{222}Rn concentration (Bq/m^3) of the hydrogeological sampling features in the study area. Types are labelled by: S spring, C cave water, D dug well

characteristics of a complex karst hydrogeological system. This analysis identified three processes controlling the hydrochemical parameters in the study area, namely dissolution of carbonate rocks, dissolution of siliciclastic rocks, and cation exchange. The geological structure also plays an essential role in shaping the groundwater flow system in the study area, as indicated by both stable (^{18}O and ^{2}H) and unstable (^{222}Rn) isotope data.

Spatial variation and hydrochemical processes

The hydrochemical characteristics of the study area show that the main processes in groups C2 and C3 are the dissolution of carbonate rocks, cation exchange, and slight dissolution of siliciclastic rocks, while in group C1, carbonate and siliciclastic rocks dissolution with limited cation exchange dominates. For the nonkarst aquifer system (group C4), the primary processes are the dissolution of siliciclastic rocks and cation exchange. The hydrochemical processes are represented by the Mg^{2+}/Ca^{2+} and Ca^{2+}/Na^{+} molar ratios, and the spatial distribution is shown in Fig. 11.

Water samples that reflect the dissolution of not only carbonate rocks but also silicate minerals are indicated by low Mg^{2+}/Ca^{2+} ratio (Narany et al. 2014; Katz et al. 1997; Thilakerathne et al. 2015). These water samples

Table 8 Range, average, standard deviation (SD) and coefficient of variance (CV) of ^{222}Rn concentrations in each type of hydrogeological feature in the study area

Hydrogeological feature/type	Lithology	*N*	^{222}Rn (Bq/m^3)	
Artesian fault-guided spring	Limestone, contact between limestone and quartz sandstone	13	Range	4,550–18,700
			Average	11,851
			SD	4,956
			CV	41.95
Cave water	Limestone, contact between limestone and calcareous sandstone	4	Range	441–19,200
			Average	10,315
			SD	7,850
			CV	76.10
Contact spring	Limestone	9	Range	3,100–14,400
			Average	7,521
			SD	3,825
			CV	50.86
Contact spring	Contact between limestone and quartz sandstone	7	Range	8,060–15,000
			Average	11,694
			SD	2,268
			CV	19.39
Dug well	Calcareous sandstone	13	Range	699–19,300
			Average	9,367
			SD	5,644
			CV	60.25
Nonkarst spring	Quartz sandstone	4	Range	7,950–17,000
			Average	13,563
			SD	4,246
			CV	31.31
Nonkarst spring	Volcanic rocks	1	Value	1,470

are mainly located in the west to the northwest of the study area, namely in the sandstone of the Wonocolo Formation, the quartz sandstone of the Ngrayong Formation, and the sites of contact between limestones and the quarts sandstones of the Ngrayong Formation. This condition is plausible because the sandstones of the Wonocolo Formation, which has calcareous properties, and the quartz sandstones of the Ngrayong Formation are both siliciclastic rocks (Luthfi et al. 2017; Novita et al. 2017). The low Mg^{2+}/Ca^{2+} ratio of springs emerging from the limestones of the Bulu Formation and the limestones of the Ledok Formation in the north and east of the study area reflects the effects of groundwater from the underlying siliciclastic rock formation. For this reason, three artesian fault-guided springs that yield the largest discharge (S-1, S-2, and S-10) and most of the other water sources are included in groups C1 and C4, which have low Mg^{2+}/Ca^{2+} ratios (< 0.4). The Mg^{2+}/Ca^{2+} ratio is around 0.5, which represents the dominance of carbonate rock dissolution (Mayo and Loucks 1995; Rajmohan and Elango 2004), particularly in springs appearing in the upper slope of the faulted hills whose lithology is composed of limestones from the Bulu Formation (S-40, S-44, and S-45) and at the bottom of the anticlinal axis at the limestones of the Tawun Formation (S-48, S-51, and S-53). Most of these springs are included in group C2. The water samples at these locations also show Mg^{2+} enrichment because they are saturated not only with calcite but also dolomite. This condition is probably related to the thickness of the limestone formation through which the groundwater in the faulted hills flows. Meanwhile, in the plunging

anticlinal hills, which are the oldest rock in the study area, the influence of groundwater from the quartz sandstones of the Ngrayong Formation is relatively nonexistent. Mg^{2+} enrichment is also present in water samples in the north area, namely a spring in volcanic rocks (S-16) and two nearby springs that are located close to the limestones of the Bulu Formation (S-55 and S-56). The Mg^{2+} enrichment in these three springs marks the influence of volcanic rocks.

The cation exchange process that is associated with Na^+ enrichment can be identified from the low Ca^{2+}/Na^+ ratio (Schoeller 1977; Hem 1992). Low Ca/Na ratio (<5) characterizes springs formed in the quartz sandstones of the Ngrayong Formation (group C4) and most of the dug wells whose lithology is composed of sandstones of the Wonocolo Formation (group C2). The Na^+ enrichment in these water sources is the consequence of intensive cation exchange between Ca^{2+} and Na^+ ions in a groundwater flow system involving slow movement through the pores. This condition occurs because the quartz sandstones of the Ngrayong Formation have many claystone intercalations, whereas the sandstone of the Wonocolo Formation has many sandy marl intercalations. A high Ca^{2+}/Na^+ ratio (>10) is exhibited in the water sources around the faults and folds (group C1), except for the springs in the southwest part of the study area, on the slopes of the faulted hills (S-44 and S-45). The high Ca^{2+}/Na^+ ratio in these water samples indicates that the cation exchange is not intensive because the water flows through fractures (geological structure). Based on the Ca^{2+}/Na^+ ratio, the cation exchange process is dominant in water sources with the lithology of the quartz sandstone of the Ngrayong Formation and the sandstone of the Wonocolo Formation.

Based on the information acquired, there are three groundwater flow systems characterized in the study area, namely the groundwater system that flows predominantly through carbonate rocks (groups C2 and C3), through siliciclastic (quartz sandstone) and volcanic rocks (group C4), and through not only carbonate rocks but also the siliciclastic rocks (quartz sandstones) below them (group C1). The high interaction between groundwater and carbonate rocks can also explain why groups C2 and C3 have higher EC, Ca^{2+}, Mg^{2+}, and HCO_3^- values and are more saturated with respect to calcite and dolomite (SIc and SId) than group C1.

Aquifer system

Referring to the concept of the Chebotarev sequence (Domenico 1972), the dominant HCO_3^- (anion) classifies the groundwater flow into an "upper zone". However, based on the $\delta^{18}O$ and δ^2H values, the groundwater flows can be divided relatively into two groups, namely shallow and deep. The aquifer systems in the study area can be categorized from the spatial variation of the stable isotope compositions using the standard equal interval method and producing a map (Fig. 12). As illustrated in the map, the $\delta^{18}O$ and δ^2H values of the water in the fault and fold zones are relatively low, representing a deep groundwater flow system. Meanwhile, the water samples of the quartz sandstones of the Ngrayong Formation and the calcareous sandstones of the Wonocolo Formation have relatively medium–to–high isotope contents, indicating a shallow groundwater flow system with a relatively slow flow and, accordingly, show the effects of the evaporation process. The result of evaporation is also manifested in the low values of d-excess, as previously explained. In addition to fault and fold zones, water samples that have low $\delta^{18}O$ and δ^2H values are mainly situated in the north, which is the highest point of the study area (above 375 masl), including S-16, S-17, S-55, and D-18. This finding shows that the groundwater system in that area is the same as that of the springs that appear in the fault and fold zones; in other words, the groundwater flow is controlled by the hydraulic gradient and geological structures.

The role of geological structure in controlling the groundwater flow system can be seen from the correlation between $\delta^{18}O$ and EC, as well as between ^{222}Rn and Cl^-, in each hierarchical group of hydrochemistry (Fig. 13). In group C1, there is no correlation between $\delta^{18}O$ and EC ($R^2 = 0.005$). In group C2, 15 out of 19 water samples (not D26, D27, S45, and C54) show a tendency of negative correlation ($R^2 = 0.45$); the higher the EC, the lower the $\delta^{18}O$ will be. In contrast, a positive correlation between the two parameters is present in group C4 ($R^2 = 0.96$). These findings show that there is almost no relationship between $\delta^{18}O$ and the duration of water–rock interaction in group C1, meaning that the geological structures control the groundwater flow system through high permeability zones. In group C2, the longer the groundwater interacts with rocks (the higher the EC value), the lower the $\delta^{18}O$, indicating that the water dominantly flows through pores. The positive correlation between EC and the $\delta^{18}O$ in group C4 is possibly attributable to the effects of the evaporation process on the shallow groundwater flow system.

Group C1 also does not show any correlation between ^{222}Rn and Cl^- in each hierarchical group of

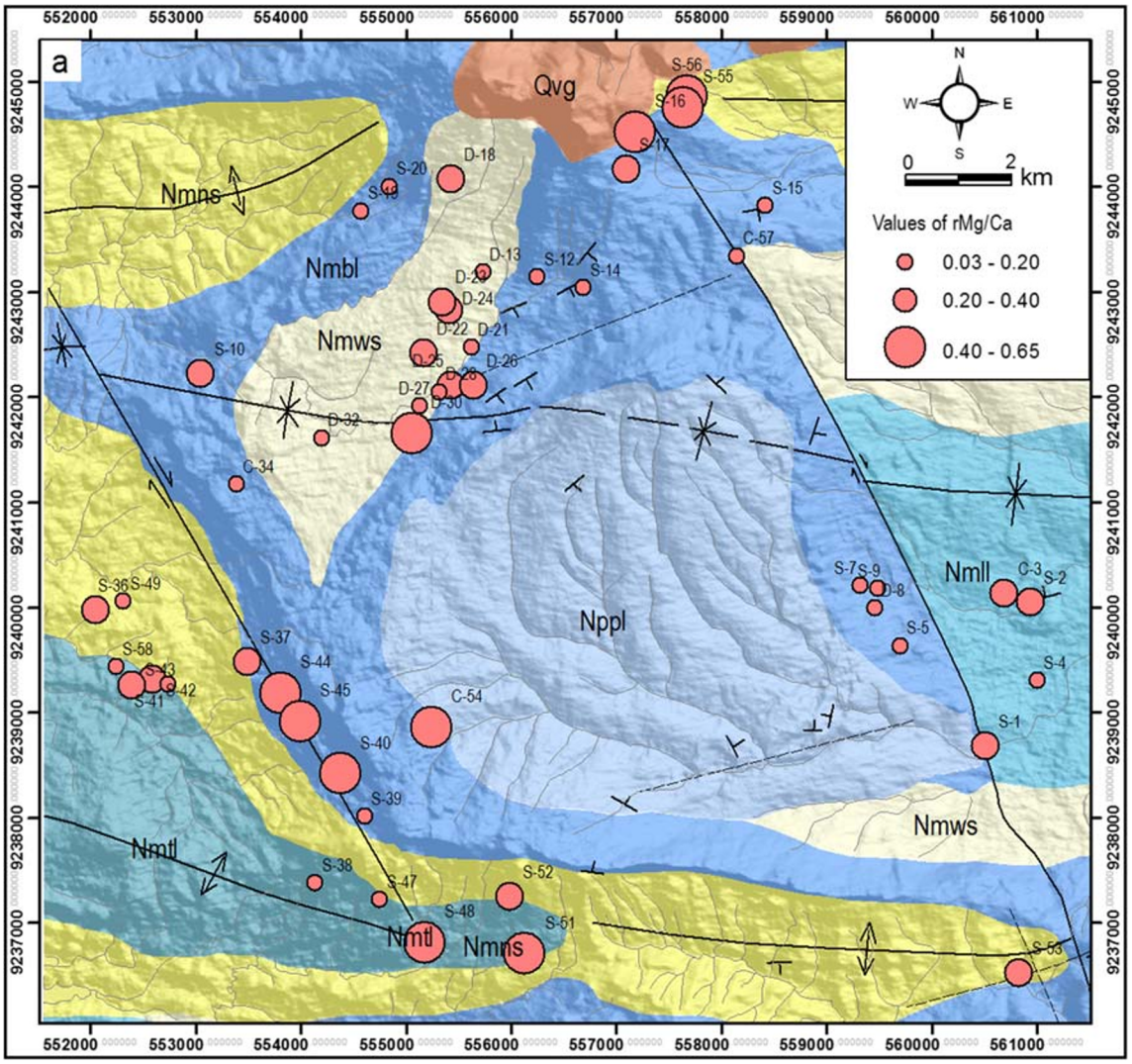

Fig. 11 Spatial distribution of the molar ratios of **a** Mg^{2+}/Ca^{2+} and **b** Ca^{2+}/Na^{+}, which represent the hydrochemical processes in the study area

hydrochemical ($R^2 = 0.035$). In group C2, 18 out of 19 groundwater samples (not S-55) show that these two parameters have a negative correlation ($R^2 = 0.34$); in other words, higher Cl^- is associated with lower ^{222}Rn concentration. Relationships with stronger values are present in three spring water samples in quartz sandstones of the Ngrayong Formation, i.e., in group C4 ($R^2 = 0.82$). The correlation indicates that the low concentrations of ^{222}Rn in groups C2 and C4 are influenced by evaporation that is associated with the relatively poor groundwater circulation associated with the springs. The significant effect of evaporation, especially in group C4 (water samples S-36 and S-49), is also shown by Cl and SO_4 enrichment; these two ions exhibit conservative behavior toward the evaporation process (Sahli et al. 2013). The absence of correlation between ^{222}Rn and Cl^- ion in group C1 suggests that the springs have active groundwater circulation because of the evolved geological structure. This condition suggests that ^{222}Rn can provide more explanation regarding the study area when applied as a tracer in fractured systems with active hydraulic character, as performed by Choubey and Ramola (1997), Cook et al. (1999), Hamada (1999), and Skeppstrom (2005).

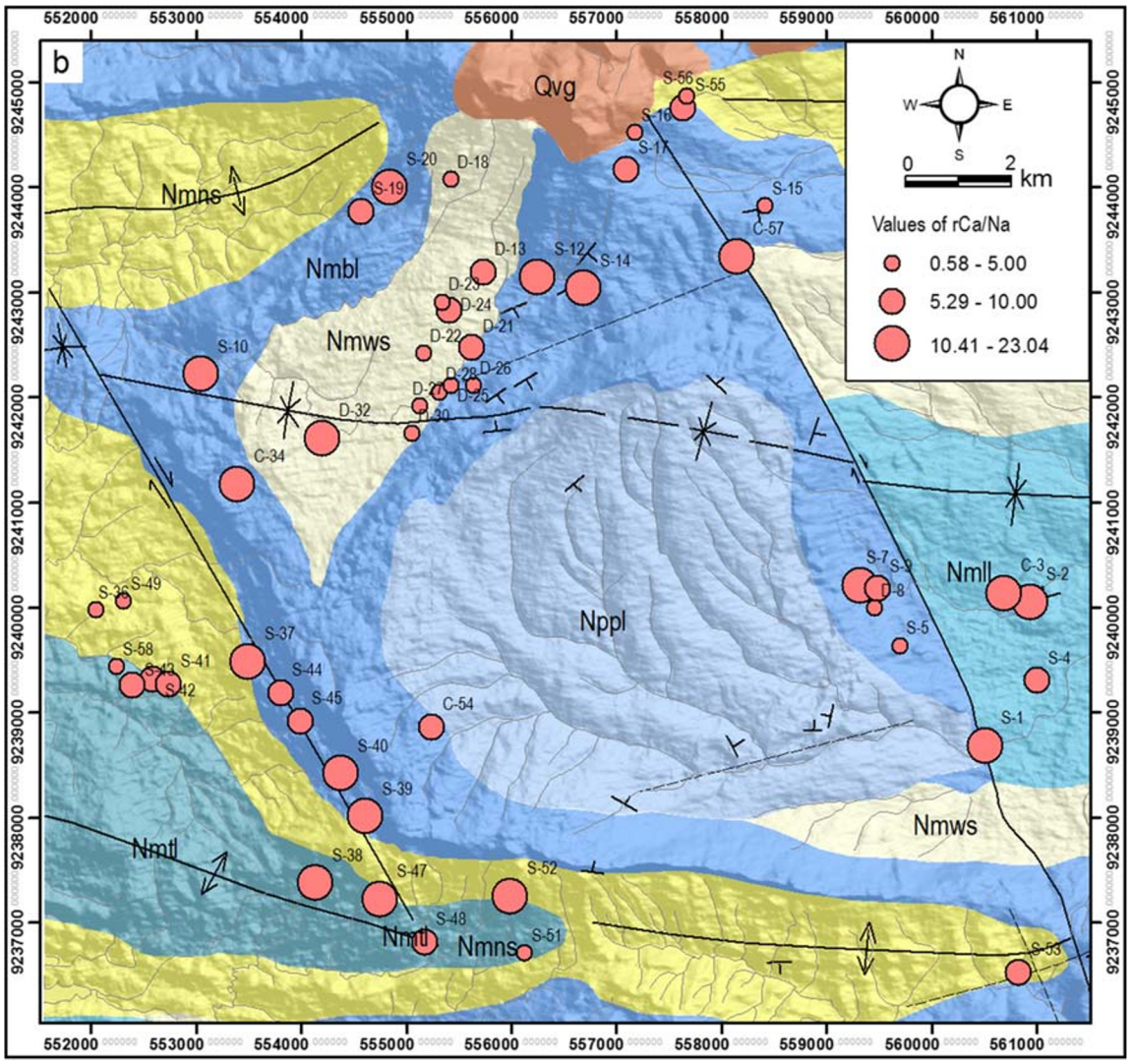

Fig. 11 continued.

The spatial variations of stable isotope composition and ^{222}Rn concentration in the different sampling features (caves, springs and wells) can also explain the complexity of the groundwater flow systems in the study area. The spring S-10, which has large discharge (95 L/s) and is located close to the west synclinal axis, has lower δ ^{18}O and δ^{2}H values than the water sources to the east, such as D-30, D-32, D-28, and D- 25. This condition indicates that S-10 is a deep groundwater flow system that is controlled by the syncline, while the hydrogeological sampling features in the east are associated with a shallow groundwater flow system. The artesian spring S-2, with the largest discharge (1,500 L/s) and located in the east synclinal limb, also has low δ ^{18}O and δ^{2}H values. Meanwhile, the artesian spring with a small discharge in the south (S-4) shows a mixing with shallow groundwater because it is located in rice fields. S-10 has a lower ^{222}Rn concentration (4,550 Bq/m^3) than the springs S-2 and S-4 (14,400 and 11,600 Bq/m^3; Fig. 10). The low concentration of ^{222}Rn in the spring S-10 is possibly attributable to the development of a cavity system in the spring outlet. The high discharge of the spring S-2 is caused by its location (i.e., the synclinal limb and at a lower elevation than the other springs) and the east–west fault system that

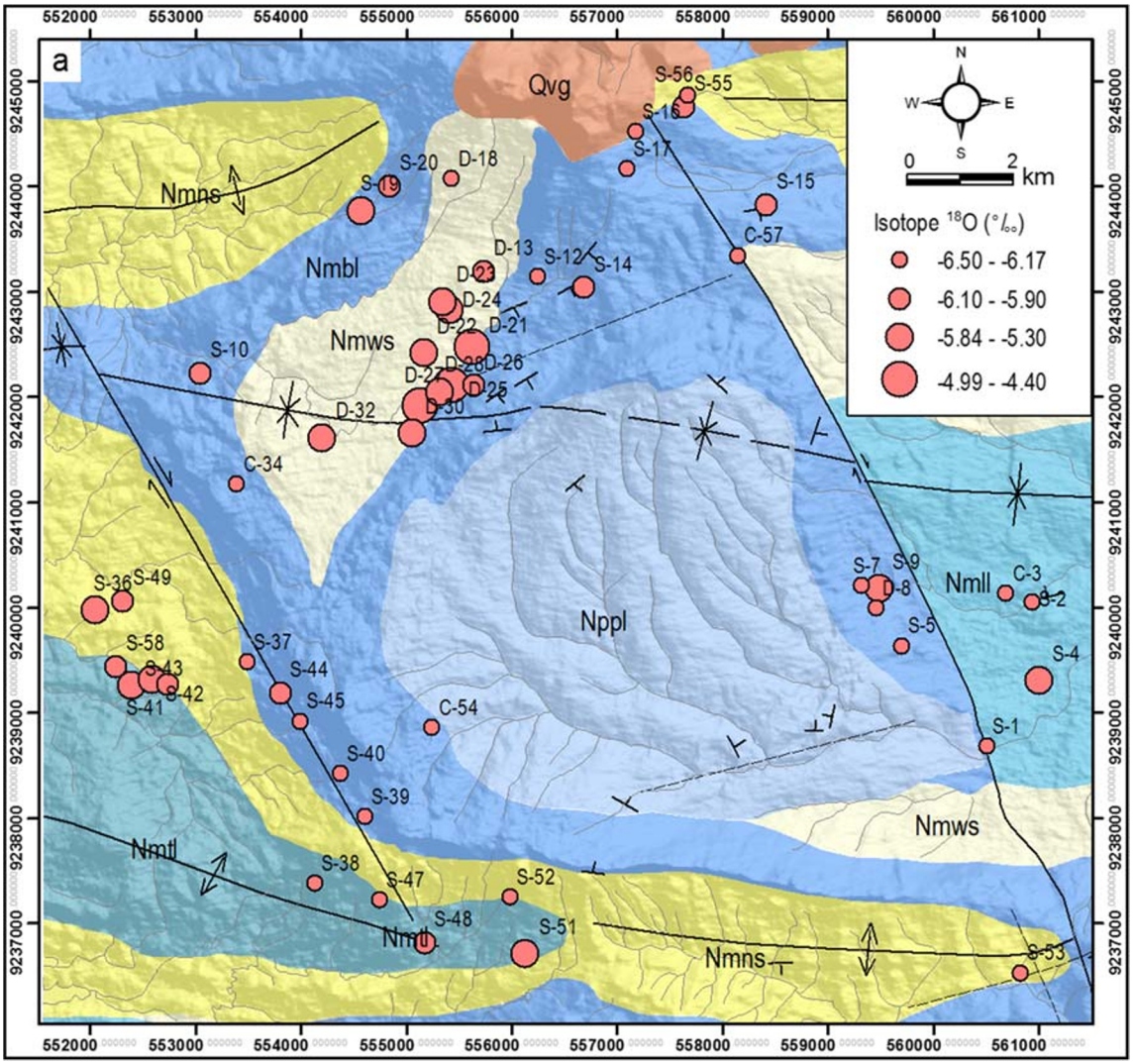

Fig. 12 Spatial distribution and classes of **a** $\delta^{18}O$ and **b** $\delta^{2}H$ values for hydrogeological sampling features in the study area

can be identified from gravity and resistivity investigation (GAI, Geological Agency of Indonesia, Jakarta, Indonesia, unpublished report, 2017).

The $\delta^{18}O$ and $\delta^{2}H$ values of the springs at the top of the plunging anticline hills such as S-38, S-47, S-52, and S-53, are relatively low, while those at the bottom of the hills such as S-48 and S-51, are relatively moderate. These conditions indicate that the springs at the top of the anticline hills originate from a deep groundwater system, whereas the ones at the bottom are mixed with shallow groundwater. The springs (S-38, S-47, and S-48) in the anticline hills whose lithology is composed of the limestones of the Tawun Formation (the oldest rock) have lower concentration of ^{222}Rn (4,490; 8,450; and 4,970 Bq/m^3) than the springs (S-51 and S-52) that are in contact with the quartz sandstones of the Ngrayong Formation (12,100 and 13,000 Bq/m^3). One spring at the peak of the faulted anticline (S-53) has a high radon concentration, that is, 18,700 Bq/m^3, due to contact with the quartz sandstone of the Ngrayong Formation (Fig. 10).

The spring S-1, which has a flow discharge of 165 L/s and is located in the normal strike-slip fault in the east, along with several of the hydrogeological sampling

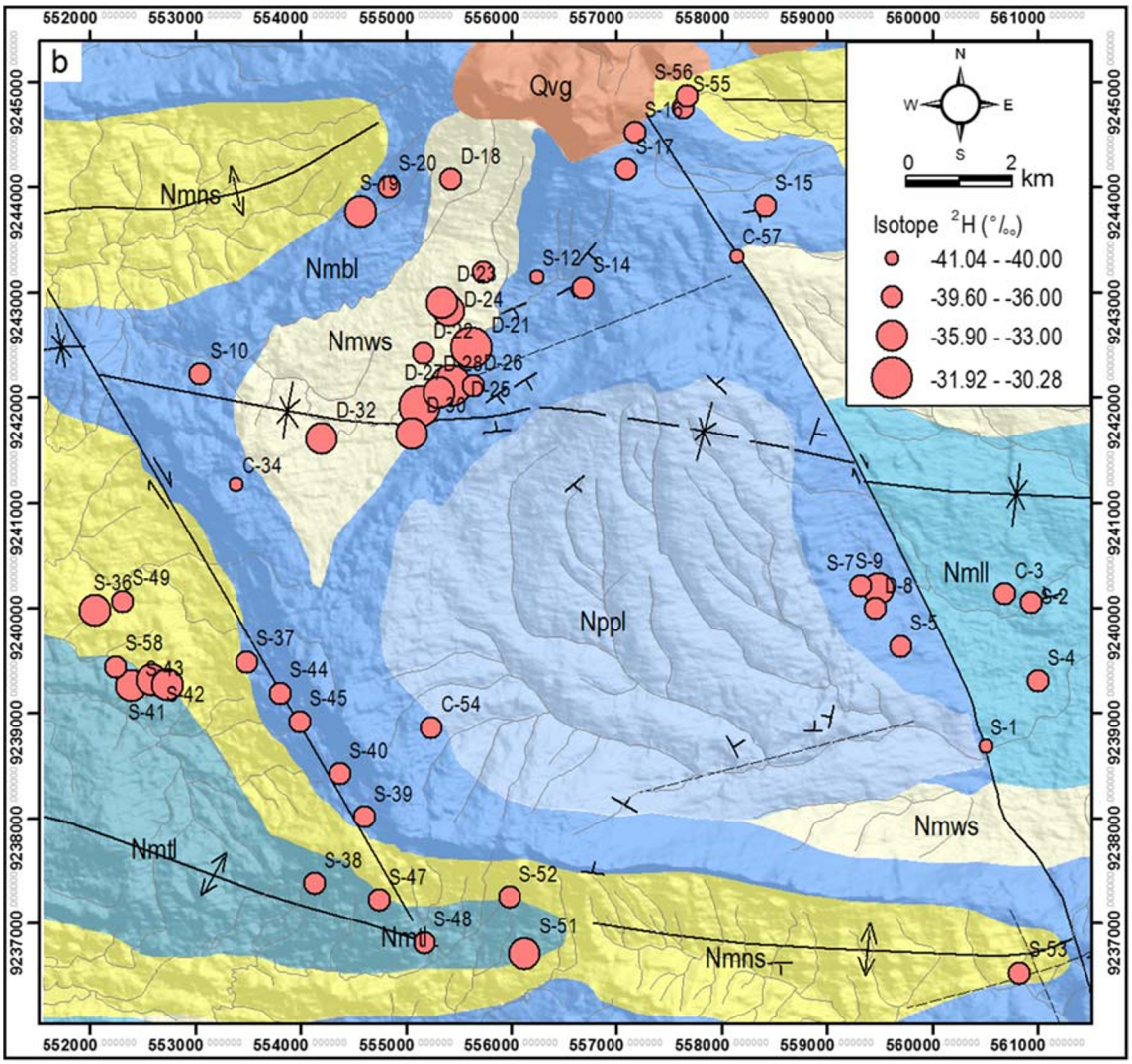

Fig. 12 continued.

features in the west of the fault (e.g., S-5, S-7, and D-8), have low δ ^{18}O and $\delta^{2}H$ values, but a high ^{222}Rn concentration is present in S-1 and S-5 (14,100 and 14,400 Bq/m^3). All springs in the part of the thrust strike-slip fault in the west (S-37, S-39, S-40, S-45, and S-44) also have low δ ^{18}O and $\delta^{2}H$ values with high levels of ^{222}Rn (11,400; 17,500; 13,400; 17,900; and 12,600 Bq/m^3, respectively; Fig. 10). In addition to the lower elevation, the spring discharge system in the east strike-slip fault is also more relatively centralized than in the west strike-slip fault. This condition is likely to yield more significant discharge in S-1 compared with the springs emerging from both fault zones even though they have one deep groundwater flow system.

Aside from the springs found around the faults and folds, the lower $\delta^{18}O$ and $\delta^{2}H$ values are also present in the sampled cave waters. The ^{222}Rn concentrations in four cave waters (C-3, C-34, C-54, and C-57) vary, i.e., 12,800; 441; 19,200; and 8820 Bq/m^3, respectively. The low ^{222}Rn concentration in C-34 is probably related to water that is stagnant or retained in the cave. In contrast, the waters are flowing in the caves C-3 and C-54, representing active water circulation. For this reason, the geological structure controls not only the groundwater system in the springs that appear in fault and fold zones

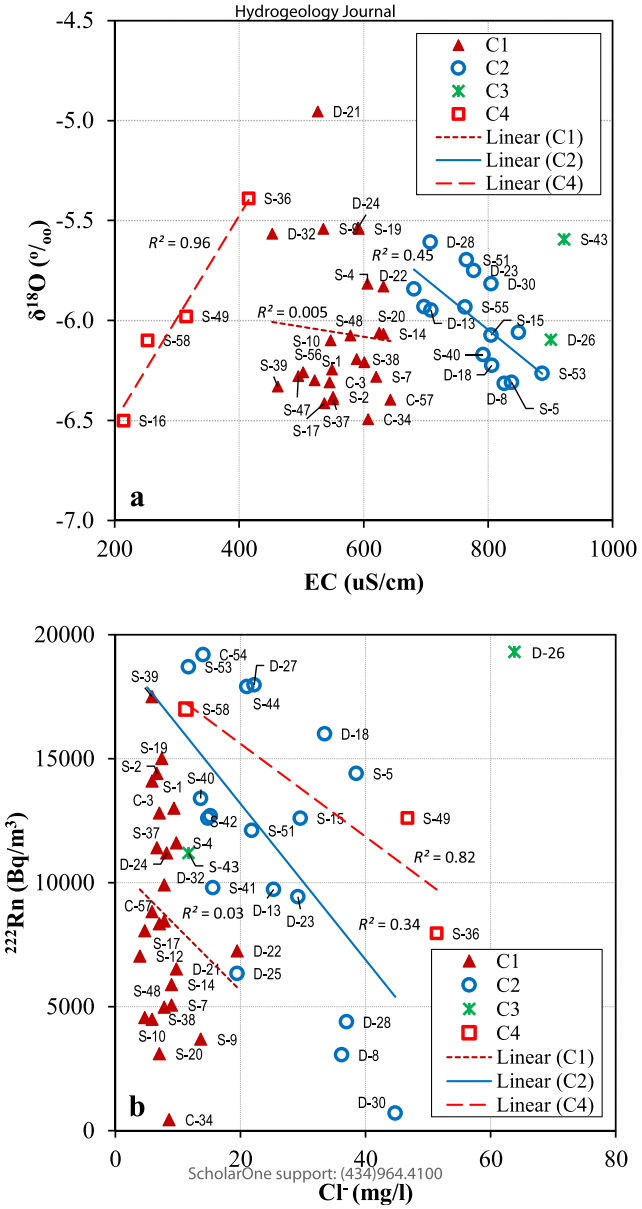

Fig. 13 Correlation between **a** $\delta^{18}O$ and EC, and **b** Cl^- and ^{222}Rn content of the water samples in the study area

but also the deep groundwater flow system connected to the cave waters. From the various descriptions above, the hydrogeological system of the study area can be simplified in a conceptual model, as depicted in Fig. 14. The subsurface conditions are reconstructed based on a geophysical survey using gravity and resistivity methods (GAI, Geological Agency of Indonesia, Jakarta, Indonesia, unpublished report, 2017).

Conclusions

The integration of hierarchical cluster analysis of hydrochemical data and environmental isotopes (^{18}O, ^{2}H, and ^{222}Rn) data has successfully identified a more comprehensive set of hydrogeological system characteristics for the study area. There are generally three groups of groundwater system that can be hydrochemically characterized, namely groundwater that flows predominantly through carbonate rocks (group C2 and C3), through siliciclastic rocks (quartz sandstone) and volcanic rocks (group C4), and through not only carbonate rocks but also the siliciclastic rocks (quartz sandstones) below them (group C1). Springs with large discharge, classified as artesian fault-guided springs, are included in group C1 such as Sumbersemen (S2), Brubulan Tahunan (S1), and Brubulan Pesucen (S10) with instantaneous discharges of 1516, 165, and 95 L/s, respectively. Based on the stable isotopes analysis, d-excess calculation, and the measurement of ^{222}Rn concentrations, the groundwater flow systems in groups C2, C3, and C4 are identified as shallow groundwater flow systems in which the groundwater flows through the pores (relatively slow). Meanwhile, group C1 is a deep groundwater flow system that is controlled by the geological structure (relatively fast flow). The geological structure not only determines the groundwater systems in springs that appear in fault and fold zones but also in cave streams. The shallow groundwater system is indicated by water that originates from local rainwater, some of which is affected by secondary evaporation processes, whereas the deep groundwater system is associated with the groundwater in the hills located in the north of the study area whose elevation is above 375 masl.

Acknowledgements Authors would like to express their deepest gratitude to the Head of the Center for Groundwater and Environmental Geology and the Head of the Geological Agency the Ministry of Energy and Mineral Resources of Indonesia for their data and laboratory facilities assistance during the research activity. Authors would also like to thank the Head of the Office of Energy and Mineral Resources Assessment and Monitoring in Kendeng Selatan for facilitating the field activities, the academic community of the Faculty of Geological Engineering UNPAD for their invaluable critiques during the writing of this report, and Ahmad Taufiq, Ph.D. for the additional discussion.

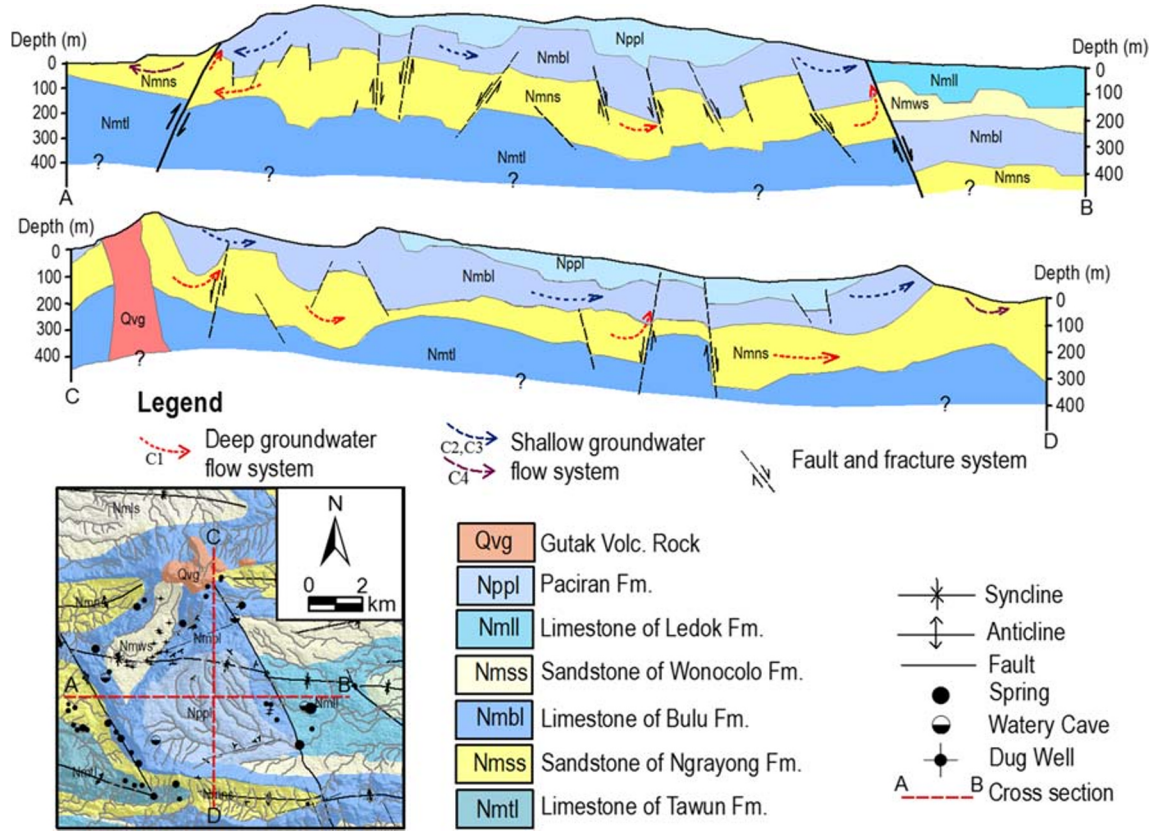

Fig. 14 The hydrogeological conceptual model of the study area that describes the aquifer system and groundwater flow in the west–east (A–B) and north–south (C–D) directions. Groups C2, C3, and C4 are shallow groundwater systems, while group C1 is a deep groundwater system

References

Al-Charideh A (2011) Geochemical and isotopic characterization of groundwater from shallow and deep limestone aquifers system of Aleppo basin (North Syria). Environ Earth Sci 65:1157–1168. https://doi.org/10.1007/s12665-011-1364-6

Al-Gamal SA (2011) An assessment of recharge possibility to North-Western Sahara aquifer system (NWSAS) using environmental isotopes. J Hydrol 398:184–190

Ashjari J, Raeisi E (2006) Lithological control on water chemistry in karst aquifers of the Zagros range, Iran. Cave Karst Sci 33:111

Belkhiri L, Mouni L, Tiri A (2011) Water-rock interaction and geochemistry of groundwater from the Ain Azel aquifer, Algeria. Environmental geochemistry and health 34:1–13. https://doi.org/10.1007/s10653-011-9376-4

Bemmelen RW (1949) The geology of Indonesia. Martinous Nijhoff, Leiden, The Netherlands

Blasch KW, Bryson JR (2007) Distinguishing sources of groundwater recharge by using δ^2H and $\delta^{18}O$. Ground Water 45:294–308

Burnett WC, Kim G, Lane-Smith D (2001) A continuous monitor for assessment of ^{222}Rn in the coastal ocean. J Radioanal Nucl Chem 249:167–172

Charfi S, Zouari K, Feki S, Mami E (2013) Study of variation in groundwater quality in a coastal aquifer in North-Eastern Tunisia using multivariate factor analysis. Quat Int 302:199–209

Chihi H, de Marsily G, Belayouni H, Yahyaoui H (2015) Relationship between tectonic structures and hydrogeochemical compartmentalization in aquifers: example of the "Jeffara de Medenine" system, south-east Tunisia. J Hydrol Reg Stud 4:410–430

Choubey VM, Ramola RC (1997) Correlation between geology and radon levels in groundwater, soil and indoor air in Bhilangana Valley, Garhwal Himalaya, India. Environ Geol 32:258–262. https://doi.org/10.1007/s002540050215

Clark I (2015) Groundwater geochemistry and isotopes. CRC, Boca Raton, FL

Clark ID, Fritz P (1997) Environmental isotopes in hydrogeology. CRC, Boca Raton, FL, 185 pp

Clever HL (1985) Solubility data series, vol 2, krypton, xenon and radon. Pergamon, Oxford

Craig H (1961) Isotopic variations in meteoric waters. Science 133:1702–1703

Cook PG, Love AJ, Dighton JC (1999) Inferring groundwater flow in fractured rock from dissolved radon. Ground Water 37(4):606–610

Coplen T (1993) Use of environmental isotopes. In: Alley WM (ed) Regional groundwater quality. Reinhold, New York, pp 227–254

Criss R, Davisson L, Surbeck H, Winston W (2007) Isotopic methods. In: Goldscheider N, Drew D (eds) Methods in karst hydrogeology. Taylor and Francis, London

Dansgaard W (1964) Stable isotopes in precipitation. Tellus 16:436–468

Davis JC (1986) Statistics and data analysis in geology. Wiley, New York

Dimitriou E, Tsintza P (2015) Hydrogeologic investigations in western Crete by using isotopic analyses and GIS techniques. J Water Resour Prot 07:923–937. https://doi.org/10.4236/jwarp.2015.712076

Domenico PA (1972) Concepts and models in groundwater hydrology. McGraw-Hill, New York

Domenico PA, Schwartz FW (1990) Physical and chemical hydrogeology. Wiley, New York

Doveri M, Menichini M, Cerrina Feroni A (2013) Stable water isotopes as fundamental tool in karst aquifer studies: some results from isotopic applications in the Apuan Alps carbonatic complexes (NW Tuscany). Ital J Eng Geol Environ 1:33–50

El-Fiky A (2010) Hydrogeochemical characteristics and evolution of groundwater at the Ras Sudr-Abu Zenima area, Southwest Sinai, Egypt. J King Abdulaziz Univ Earth Sci 21:79–109. https://doi.org/10.4197/Ear.21-1.4

Falcone RA, Falgiani A, Parisse B, Petitta M, Spizzico M, Tallini M (2008) Chemical and isotopic ($^{18}O‰$, $^{2}H‰$, $^{13}C‰$, ^{222}Rn) multitracing for groundwater conceptual model of carbonate aquifer (Gran Sasso INFN Underground Laboratory, central Italy). J Hydrol 357:368–388. https://doi.org/10.1016/j.jhydrol.2008.05.016

Ford D, Williams PW (1989) Karst geomorphology and hydrology. Chapman and Hall, London

Ford D, Williams PW (2007) Karst hydrogeology and geomorphology, revised edn. Wiley, Chichester, UK

Freeze RA, Cherry JA (1979) Groundwater. Prentice Hall, Upper Saddle River, NJ

Gat JR (1980) The isotopes of hydrogen and oxygen in precipitation. In: Fritz P, Fontes JC (eds) Handbook of environmental isotope geochemistry. Springer, Berlin, pp 21–47

Gat JR, Bowser CJ, Kendall C (1994) The contribution of evaporation from the Great Lakes of North America to the continental atmospheric moisture: detection by means of the stable isotope signature of the evaporated waters. Geophys Res Lett 20:557–560

Gibson J, Briks S, Edwards T (2008) Global prediction of δ_A and δ^2H–$\delta^{18}O$ evaporation slopes for lakes and soil water for seasonality. Glob Biogeochem Cycles 22:1–12

Goldscheider N, Andreo B (2007) The geological and geomorphological framework. In: Goldscheider N, Drew D (eds) Methods in karst hydrogeology. Taylor and Francis, London

Goldscheider N, Drew D, Worthington S (2007) Introduction. In: Goldscheider N, Drew D (ed) Methods in karst hydrogeology. Taylor and Francis, London

Guler C, Thyne DG (2004) Hydrologic and geologic factors controlling surface and groundwater chemistry in Indian Wells-Owens Valley area, southeastern California. USA J Hydrol 285:177–198

Guler C, Thyne GD, McCray JE, Turner AK (2002) Evaluation of graphical and multivariate statistical methods for classification of water chemistry data. Hydrogeol J 10:455–474

Hamada (1999) Estimation of groundwater flow rate using the decay of ^{222}Rn in a well. J Environ Radioact 47:1–13

Harvey F (2001) Use of NADP archive samples to determine isotope composition of precipitation: characterizing the meteoric input function for use in ground water studies. Ground Water 39(3):380–390

Haryono E (2001) Values of the karst hills. Paper presented at The National Seminar of Eco-Hydraulics, Gadjah Mada University, Yogyakarta, Indonesia, 28–29 March 2001

Hem JD (1992) Study and interpretation of the chemical characteristics of natural waters. US Geol Surv Water Suppl Pap 1473, pp 269

Iskandar I, Dermawan FA, Sianipar JY, Suryantini NS (2018) Characteristic and mixing mechanisms of thermal fluid at the Tampomas volcano, West Java, using hydrogeochemistry, stable isotope and ^{222}Rn analyses. Geosciences 2018(8):103. https://doi.org/10.3390/geosciences8040103

Jankowski J (2001) Groundwater environment. Short course note, School of Geology, University of New South Wales, Sydney

Katz BG, Coplen TB, Bullen TD, Davis JH (1997) Use of chemical and isotopic tracers to characterize the interactions between ground water and surface water in mantled karst. Ground Water 35:1014–1028. https://doi.org/10.1111/j.1745-6584.1997.tb00174.x

Kehew AE (2001) Applied chemical hydrogeology. Prentice Hall, Upper Saddle River, NJ

Kendall C, McDonnell JJ (1998) Isotopes tracers in catchment hydrology. Elsevier, Amsterdam

Krishnaraj S, Murugesan VKV, Sabarathinam C, Paluchamy A, Ramachandran M (2012) Use of hydrochemistry and stable isotopes as tools for groundwater evolution and contamination investigations. J Geosci 1:16–25. https://doi.org/10.5923/j.geo.20110101.02

Leibundgut C, Maloszewski P, Külls C (2009) Tracers in hydrology. Wiley-Blackwell, Hoboken, NJ

Li J, Liu J, Pang Z, Wang X (2013) Characteristics of chemistry and stable isotopes in groundwater of the Chaobai River catchment, Beijing. Procedia Earth Planet Sci 7:487–490. https://doi.org/10.1016/j.proeps.2013.03.092

Luthfi M, Kudsji DK, Maryanto S, Supriyono (2017) Geological map of the Jatirogo quadrangle, scale of 1:50000. Center for Geological Survey, Geological Agency of Indonesia, Bandung, Indonesia

Machavaram MV, Krishnamurthy RV (1995) Earth surface evaporative process: a case study from the Great Lakes region of the United States based on deuterium excess in precipitation. Geochim Cosmochim Acta 59:4279–4283

Mahlknecht J, Garfias-Solis J, Aravena R, Tesch R (2006) Geochemical and isotopic investigations on groundwater residence time and flow in the Independence Basin, Mexico. J Hydrol 324:283–300

Marfia AM, Krishnamurthy RV, Atekwana EA, Panton WF (2004) Isotopic and geochemical evolution of groundwater and surface waters in a karst-dominated geological setting: a case study from Belize, Central America. Appl Geochem 19:937–946. https://doi.org/10.1016/j.apgeochem.2003.10.013

Mayo AL, Loucks MD (1995) Solute and isotopic geochemistry and ground water flow in the Central Wasatch Range, Utah. J Hydrol 172:31–59. https://doi.org/10.1016/0022-1694(95)02748-e

Merlivat L, Jouzel J (1979) Global climatic interpretation of deuterium-oxygen relationship for precipitation. J Geophys Res 84:5029–5033

Michel J (1990) Relationship of radium and radon with geological formations. In: Cothern CR, Rebers PA (eds) Radon, radium, and uranium in drinking water. Lewis, Chelsea, MI, 286 pp

Milanovic PT (1981) Karst hydrogeology. Water Resources Publ., Littleton, CO

Mukherjee A, Fryar AE, Rowe HD (2007) Regional-scale stable isotopic signatures of recharge and deep groundwater in the arsenic affected areas of West Bengal, India. J Hydrol 334:151–161

Murillo RS, Brooks E, Elliot JW, Bolla J (2015) Isotope hydrology and baseflow geochemistry in natural and human-altered watersheds in the inland Pacific Northwest, USA. Isot Environ Health Stud 51:231–254. https://doi.org/10.1080/10256016.2015.1008468

Narany ST, Ramli MF, Aris AZ, Sulaiman WNA, Juahir H, Fakharian K (2014) Identification of the hydrogeochemical processes in groundwater using classic integrated geochemical methods and geostatistical techniques in Amol-Babol plain, Iran. Sci World J 2014:1–15. https://doi.org/10.1155/2014/419058

Novita D, Margono U, Sanjaya I, Rijani S (2017) Geological map of the Blora quadrangle, scale of 1:50000. Center for Geological Survey, Geological Agency of Indonesia, Bandung, Indonesia

Parkhust DL, Appelo CAJ (1999) User's guide to Phreeqc (version 2) – a computer program for speciation, batch-reaction, one-dimensional transport, and inverse geochemical calculations. US Geological Survey, Reston, VA

Petitta M, Primavera P, Tuccimei P, Aravena R (2011) Interaction between deep and shallow groundwater systems in areas affected by Quaternary tectonics (central Italy): a geochemical and isotope approach. Environ Earth Sci 63:11–30. https://doi.org/10.1007/s12665-010-0663-7

Pu T, He Y, Zhang T, Wu J, Zhu G, Chang L (2013) Isotopic and geochemical evolution of ground and river waters in a karst dominated geological setting: a case study from Lijiang basin, South-Asia monsoon region. Appl Geochem 33:199–212

Przylibski TA (2005) Radon, specific component of medicinal waters in the Sudety Mountains. Oficyna Wydawnicza Politechniki Wrocławskiej, Wrocław, Poland

Rademacher LK, Clark JF, Boles JR (2003) Groundwater residence times and flow paths in fractured rock determined using environmental tracers in the Mission tunnel: Santa Barbara County, California, USA. Environ Geol 43:557–567

Rajmohan N, Elango L (2004) Identification and evolution of hydrogeochemical processes in the groundwater environment in an area of the Palar and Cheyyar River basins, South India. Environ Geol 46(1): 47–61

Rodgers P, Soulsby C, Waldron S, Tetzlaff D (2005) Using stable isotope tracers to assess hydrological flow paths, residence times and landscape influences in a nested mesoscale catchment. Hydrol Earth Syst Sci 9:139–155

Ryu JS, Lee KS, Chang HW (2007) Hydrogeochemical and isotopic investigations of the Han River basin, South Korea. J Hydrol 345: 50–60

Sahli H, Tagorti MA, Tlig S (2013) Groundwater hydrochemistry and mass transfer in a stratified aquifer system (Jefara–Gabes Basin, Tunisia). Larhyss J 12:95–108

Savoy L (2007) Storage, transport and biodegradation of solute contaminants in the unsaturated zone of karst systems. PhD Thesis, University of Neuchâtel, Switzerland

Schoeller H (1977) Geochemistry of groundwaters. In: Ground-water studies: an international guide for research and practice. UNESCO, Paris, pp 1–18

Singh M, Kumar S, Kumar B, Singh S, Singh IB (2013) Investigation on the hydrodynamics of ganga alluvial plain using environmental isotopes: a case study of the Gomati River basin, northern India. Hydrogeol J 21:687–700

Skeppstrom K (2005) Radon in groundwater- influencing factors and prediction methodology for a Swedish environment. Licentiate Thesis, Universitetsservice US AB, Stockholm

Sun Z, Ma R, Wang Y, Ma T, Liu Y (2016) Using isotopic, hydrogeochemical-tracer and temperature data to characterize recharge and flow paths in a complex karst groundwater flow system in northern China. Hydrogeol J 24:1393–1412. https://doi.org/10.1007/s10040-016-1390-2

Swanson SK, Bahr JM, Schwar MT, Potter KW (2001) Two-way cluster analysis of geochemical data to constrain spring source waters. Chem Geol 179:73–91

Thilakerathne A, Schüth C, Chandrajith R (2015) The impact of hydrogeological settings on geochemical evolution of groundwater in karstified limestone aquifer basin in Northwest Sri Lanka. Environ Earth Sci 73:8061–8073. https://doi.org/10.1007/s12665-014-3962-6

Tillman FD, Oki DS, Johnson AG, Barber LB, Beisner KR (2014) Investigation of geochemical indicators to evaluate the connection between inland and coastal groundwater systems near Kaloko-Honoko-hau National Historical Park, Hawai'i. Appl Geochem 51: 278–292. https://doi.org/10.1016/j.apgeochem.2014.10.003

Valdes D, Dupont JP, Laignel B, Ogier S, Leboulanger T, Mahler BJ (2007) A spatial analysis of structural controls on karst groundwater geochemistry at a regional scale. J Hydrol 340:244–255. https://doi.org/10.1016/j.jhydrol.2007.04.014

Villalobos MR, Muños AC, Álvarez AP, Collado GM (2017) Hydrochemistry and ^{222}Rn concentrations in spring waters in the arid zone El Granero, Chihuahua, Mexico. Geosciences 7:12

White WB (2015) Chemistry and karst. Acta Carsol 44:349

Wu J, Li P, Qian H, Duan Z, Zhang X (2013) Using correlation and multivariate statistical analysis to identify hydrogeochemical processes affecting the major ion chemistry of waters: a case study in Laoheba phosphorite mine in Sichuan, China. Arab J Geosci. https://doi.org/10.1007/s12517-013-1057-4

Yidana SM, Banoeng-Yakubo B, Akabzaa TM (2010) Analysis of groundwater quality using multivariate and spatial analyses in the Keta basin, Ghana. J Afr Earth Sci 58:220–234. https://doi.org/10.1016/j.jafrearsci.2010.03.003

Yidana SM, Banoeng-Yakubo B, Akabzaa TM, Asiedu D (2011) Characterization of the groundwater flow regime and hydrochemistry of groundwater from the Buem formation, eastern Ghana. Hydrol Process 25:2288–2301. https://doi.org/10.1002/hyp.7992

Yuan J, Xu F, Deng G, Tang Y, Li P (2017) Hydrogeochemistry of shallow groundwater in a karst aquifer system of Bijie City, Guizhou Province. Water 9:625. https://doi.org/10.3390/w9080625

Zuppi GM (1981) Statistical treatment of environmental isotope data in precipitation. Technical Reports Series, vol 206, IAEA, Vienna